Observation of the Coastal Areas, Estuaries and Deltas from Space

Benoit Laignel[1] · Stefano Vignudelli[2] · Rafael Almar[3] · Mélanie Becker[4] ·
Abderrahim Bentamy[5] · Jérôme Benveniste[6] · Florence Birol[3] · Frédéric Frappart[7] ·
Deborah Idier[8] · Edward Salameh[1] · Marcello Passaro[9] · Melisa Menende[10] ·
Marc Simard[11] · Emma Imen Turki[1] · Charles Verpoorter[12]

Abstract

Coastal regions (including estuaries and deltas) are very complex environments with diverse hydrodynamic and bio-geomorphological contexts and with important socio-economic and ecological problems. These systems are among the most affected by human impact through urbanization and port activities, industrial and tourism activities. They are directly affected by the impact of climate change on sea level, storm surges frequency and strength, as well as recurrence of coastal river floods. A sustainable future for coastal zones depends on our capacity to implement systematic monitoring with focus on: (1) forcings affecting coastal zones at different spatio-temporal scales (sea level rise, winds and waves, offshore and coastal currents, tides, storm surges, river runoff in estuaries and deltas, sediment supply and transport, vertical land motions and land use); (2) morphological response (e.g., shoreline migration, topographical changes). Over the last decades, remote sensing observations have contributed to major advances in our understanding of coastal dynamics. This paper provides an overview of these major advances to measure the main physical parameters for monitoring the coastal, estuarine and delta environments and their evolution, such as the water level and hydrodynamics near the shoreline, water/sediment contact (i.e., shoreline), shoreline position, topography, bathymetry, vertical land motion, bio-physical characteristics of sediments, water content, suspended sediment, vegetation, and land use and land cover.

✉ Stefano Vignudelli
    stefano.vignudelli@pi.ibf.cnr.it

Extended author information available on the last page of the article

Article Highlights

- The coastal areas (including the estuaries and deltas) are very complex environments with diverse hydrodynamic and bio-geomorphological contexts and with important socio-economic and ecological issues
- A sustainable future for coastal zones depends on our capacity to implement a systematic monitoring on forcing factors and coastal responses
- Satellite-based observations using different techniques (Optical imagery; Altimetry, Microwave radar, Interferometric Synthetic Aperture Radar, Infrared, etc.) have provided major advances in coastal dynamics with the measurement of different physical quantities

1 Introduction

There are several definitions of the coastal zone and, according to these definitions, the coast can extend from a few hundred meters to several kilometers on either side of the land-sea interface, and can include the continental shelf, the littoral zone (a narrow strip located ~ 2 to 5 km from the shoreline), the nearshore, deltas and estuaries. Thus, coastal systems, located at the land-sea buffer zone, are very complex environments with diverse hydrodynamic, morphological, sedimentological, and biological contexts: coastline with cliffs, beaches with sand, mud, gravel, or pebbles, sand dunes, lagoon, bay, but can also present smoother, but very dynamic, transitions with freshwater inflow from estuaries, deltas, coastal marshes, swamps, and wetlands.

These environments are influenced by significant water level variations controlled by coastal and offshore currents, upwelling and downwelling, waves (with run-up and overtopping), tides, storm surges, river and groundwater flow, sea level rise, and vertical land movement. The combined effects of these complex phenomena on the spatial and temporal variation of water levels and their impacts on flooding patterns and morphological changes in coastal and estuarine regions are not well known and are therefore difficult to model. This is largely due to the paucity of in situ water level observations. Despite this, the spatial variability of hydrodynamics is generally studied by numerical simulations using modeling tools, as well as by field studies dedicated to specific regions and processes.

In addition, coastal environments face major economic and ecological challenges. Coastal areas are used for fishing, aquaculture, mineral extraction, industrial development, energy production, tourism and recreation, as well as for waste disposal. Estuaries are partially enclosed areas of water on the coast where salt water from the sea mixes with fresh water from rivers and streams. These transitional waters are highly biologically productive ecosystems and perform many other important ecological functions. For example, deltas, composed of huge masses of nutrient-rich sediment deposited at the mouths of large rivers, are among the most fertile regions in the world. These flat agricultural lands, which make up less than 1% of the world's land, are critical to the food security of more than half a billion people (Giosan et al. 2014). In addition, ecosystems such as coastal wetlands provide critical ecosystem services, such as supporting fisheries by providing important spawning grounds, filtering pollutants and contaminants from coastal waters, and protecting coastal developments and communities from storms, flooding, and erosion. However, the role of intertidal wetlands in regulating water flows and mass exchange (i.e., nutrients, carbon, salt) at the coastal boundary on a regional scale remains unknown.

Coastal areas are considered one of the environments most affected by human impact and climate change. These systems are subject to widespread human use, with high population density and significant port, industrial and tourism activities. In fact, few coasts in the

world today escape the influence of anthropogenic pressures, although not all coasts are inhabited (Buddemeier et al. 2002). This pressure increased dramatically during the twentieth century, a trend that appears likely to continue into the twenty-first century. Coastal population growth in many of the world's deltas, barrier islands, and estuaries has resulted in widespread conversion of natural coastal landscapes to agriculture, aquaculture, forestry, and industrial and residential development (Valiela 2006). It has been estimated that 23% of the world's population lives both within 100 km of the coast and within 100 m above sea level, and that population densities in coastal regions are about three times the global average (Small and Nicholls 2003). Direct impacts include drainage of coastal wetlands, deforestation and reclamation, and the discharge of wastewater, fertilizers, and contaminants into coastal waters. Engineering works, such as dams, channelization, and detour of coastal streams, harden the coast, alter circulation patterns, and alter the supply of freshwater, sediment, and nutrients. Natural systems are often directly or indirectly altered, even by soft engineering solutions such as beach nourishment and foredune construction (Hamm and Stive 2002). Thus, coastal ecosystem services are often disrupted by human activities.

In addition, coasts and estuaries are strongly affected by climate change, including sea level rise and increases in the intensity and occurrence of extreme events (such as storm surges, coastal river flooding, flooding) in some regions (IPCC 2014, 2021). Large waves generated by ocean storms also cause a rise in water level (setup) and generate a large run-up (e.g., Senechal et al. 2011) that can result in significant flooding. In addition, there can be strong interactions between tide, storm surge, waves, sea level rise, and flooding (Idier et al. 2019), which adds an additional level of complexity. In fact, there is a combination of several processes that can lead to very significant flooding if these processes occur at the same time: storm surge, wave, high tide, coastal river inundation, groundwater inundation, and sea level rise. On the other hand, many of the world's coastlines are eroding and therefore retreating. For example, by the end of the century, nearly half of the world's sandy beaches could disappear almost entirely due to human-induced erosion exacerbated by climate change (Vousdoukas et al. 2020). In the delta example, the combination of sea level rise, subsidence, shoreline retreat, sediment starvation, and extreme weather events, coupled with rapid population growth and increasing human impact on river basins and natural resources, threatens delta communities (IPCC 2019). These effects are likely to be dominant in the twenty-first century. In addition to erosion and flood damage, these environments are subject to significant changes in water quality especially during extreme floods, with increased turbidity from the river to the sea; this creates a turbidity plume affecting the hydrodynamic conditions of tidal currents and waves in coastal areas.

In summary, the consequences of human impact and climate change in these environments are numerous, diverse and important, and are defined as multiple risk areas: flooding, erosion (retreat of the coastline), morphological and sedimentary change, change in water quality (pollution), property damage, reduction of beach area and on tourism. As a result, the design and management of coastal infrastructure (harbors, dikes, etc.) as protection against the sea must be reviewed, with considerable costs. According to the Organisation for Economic Co-operation and Development (OECD 2005), the material damage to coasts affected by hydro-meteorological phenomena in 2005 was estimated at 3000 billion dollars (5% of the world's annual GDP) and could increase tenfold by 2070.

A sustainable future for coastal areas depends on our ability to monitor hydrodynamics, including quantifying current rates of sea level rise and vertical land movement, but also to monitor the morphology, sedimentology, and biology of these diverse environments that are impacted by a variety of natural and anthropogenic environmental changes. This monitoring must include different scales of time and space, in order to understand, predict and manage

the evolution of these environments. Satellite data are based on different techniques (optical imagery, altimetry, microwave radar, interferometric synthetic aperture radar, infrared, etc.) allowing to measure different physical quantities. In order to find the best compromise between coverage and spatial, temporal and spectral resolution for the monitoring of coastal environments, a multi-sensor approach must be favored. Key spatially derived physical parameters for monitoring coastal and estuarine environments and their evolution include water level and hydrodynamics, water/sediment contact (i.e., shoreline), shoreline position, topography, bathymetry, vertical soil movement, biophysical characteristics of sediments, water content, suspended sediments, vegetation, land use and cover.

2 Hydrodynamics in the Coastal Areas

As already specified above, coastal environments are affected by large variations in water levels, controlled by offshore currents, wind-induced shelf circulation, waves, tides, storm surges, sea level rise, and stream and groundwater flow. Remote sensing observations provide essential information on the spatial variability of water surface elevations under different hydrodynamic conditions. Over the past two decades, satellite radar altimeters, measuring sea level variations, have provided major advances in ocean dynamics (Fu and Chelton 2001; Stammer and Cazenave 2018) but have encountered numerous problems in coastal environments, resulting in rapid degradation of data accuracy as they approach the coast. In addition, nadir altimetry missions, such as the TOPEX/POSEIDON and Jason series, have inter-track spacing and temporal resolution that limit their ability to map smaller-scale coastal features, such as shelf tides, coastal tides, wind effects, and storm surges (Arbic et al. 2014). However, the upcoming NASA/CNES SWOT mission, to be launched in 2022, will cover nearly the entire ocean surface with an unprecedented spatial resolution of 1 km and with revisit ranging from 2 (at the equator) to 7 (at high latitudes) times per 21-day cycle (Morrow et al 2019), will provide a new perspective for measuring sea level and for better understanding hydrodynamics (and the interactions between offshore currents, wind-driven shelf circulation, waves, tides, storm surges, sea level rise, and stream and groundwater flow on water level) in coastal areas.

As one approaches the coast, the major challenge with radar altimetry is that the models used to adjust the recovered echoes and derive the geophysical parameters to be applied to the altimeter measurements assume that the orientation of the scatterers illuminated by the pulse hitting the sea surface is randomly distributed (Brown 1977). This is not always true in the coastal zone: due to the size of the radar footprint, spurious returns from land elevated at the coast or mirror reflections from the water (e.g., due to sheltered areas) are present in the received echoes (Gómez-Enri et al. 2010). The sea area affected by these signal disturbances can vary considerably depending on the type of coastline, sea state, and altimeter used, but generally extends to about 10–15 km from the coast. Even with the latest signal processing techniques in modern radar altimetry (i.e., unfocused and fully focused Delay-Doppler altimeters), the focusing of the echo and the consequent reduction of the footprint represented in an altimeter waveform is concerned with the along-track dimension, but not the cross-track dimension (Scagliola 2013). Nevertheless, the adoption of dedicated signal adjustment strategies can largely solve this problem, especially increasing the amount of valid retrievals up to the coast (Passaro et al. 2014).

A second challenge for coastal altimetry is the adoption of specific corrections to account for the delay of the radar echo passing through the atmosphere and reaching the

sea surface. Delays caused by interaction with the atmosphere can be corrected by comparing range measurements at different frequencies (for ionospheric delays) or by using radiometer measurements (for tropospheric delays). In both cases, these techniques are affected by the presence of land (Fernandes et al. 2014). Delays can also be derived using modeled data, which may nevertheless have suboptimal spatial and temporal resolution. This is particularly the case for the delay caused by water vapor (called the wet troposphere correction). However, combined solutions using radiometric measurements, in-situ measurements from coastal stations and modeled data now exist (Lázaro et al. 2020; Fernandes et al. 2021).

Measuring sea level in the coastal zone also means dealing with more complex spatial and temporal scales of variability than in the open ocean. A typical example is the ocean tide, which is not temporally resolved by altimetry and must be removed from the instantaneous altimeter measurements to avoid the tide signal being aliased into the ocean topography. This is done by using sea level estimates provided by tidal models. Coastal boundaries and bathymetry variations intensify the tidal signal and generate internal tides that are difficult to predict with hydrodynamic models. Moreover, for the reasons explained above, the use of satellite altimetry to improve tidal models is limited by the coastal performance of the altimetry measurement itself. Improvements in coastal altimetry data (Piccioni et al. 2018), local knowledge of bathymetry (Cancet et al. 2019; Rasquin et al. 2020), and internal tidal calculations (Ray and Zaron 2011) significantly improve the quality of tidal models in the coastal zone, and thus the exploitation of sea level altimetry data for other types of applications.

Wind waves also affect the reflected altimeter signal, which is used to estimate the significant wave height (SWH, the average height of the highest third of the waves illuminated by the satellite footprint). Note that the significant wave height is not affected by atmospheric delays and therefore improvements in the adjustment strategy in coastal areas lead to a direct increase in the quality of its retrievals in these areas. Shallow-water waves are subject to rapid changes due to coastal bottom topography (Dodet et al. 2019), but their measurement is necessary to assess the impact of sea level rise at the coast in terms of total water level (Melet et al. 2018). In addition, the correct estimation of SWH is critical for the accuracy of sea level data due to the interaction of the wave field with the radar echo, which is accounted for in the sea state bias correction (Tran et al. 2010).

Finally, even using the most advanced processing techniques mentioned above, altimetry in the coastal zone requires a dedicated approach. At the global scale, the use of altimetry relies mainly on the generation of mesh products with a resolution typically of ¼°, combining available multi-mission data, but with large-scale filtering along the track and strong interpolation in space and time (Pujol et al. 2016; Legeais et al. 2018, CMEMS, C3S). This hinders the ability to observe coastal variability at small scales and smoothes out changes in ocean variability toward the coast. Direct use of data along the trace of consecutive runs can be used locally to circumvent this problem (Birol et al. 2010), but is of limited value relative to typical user needs. The recent rapid increase in the number of altimetry satellites orbiting simultaneously and the evolution of altimetry measurement from a one-dimensional profile to a two-dimensional swath (Fu and Ubelmann 2014) are promising advances that will aid in the production of seamless sea level estimates suitable for coastal stakeholders. In addition, monitoring the coastal zone with satellite altimetry is now a requirement of the most recent missions (Scharroo et al. 2016). The critical need to use radar altimetry in the coastal zone has fostered tremendous improvements in recent years and now allows for accurate measurements to within 5 km of the coast of several processes such as sea level, current, waves, and wind and storm surges (Benveniste et al. 2019).

2.1 Sea Level Measurement

Coastal sea level has historically been observed using in-situ data. These are collected by a network of tide gauges, whose distribution is nevertheless extremely uneven over the globe (Permanent Service for Mean Sea Level, Holgate et al. 2013). For this reason, one of the main interests of calculating coastal sea level from altimetry is to provide measurements in areas that are not sampled by in-situ measurements. Tide gauges are also used to calibrate and validate measurements from satellite altimetry (Leuliette et al. 2004; Nerem and Mitchum 2001). This process is also enhanced by the availability of better altimetry data in the coastal zone.

There are important differences to consider when comparing sea level measurements from satellite radar altimetry and tide gauges. First, satellite radar altimetry measures absolute sea level, relative to a reference surface (the ellipsoid or geoid), whereas tide gauges measure sea level relative to the land and are subject to the vertical motions of the land (Wöppelmann and Marcos 2016). Second, altimeter data are typically provided to users as absolute sea surface height (SSH), i.e., corrected for the contribution of atmospheric pressure and ocean tide and loading, whereas tide gauge measurements are typically provided in terms of total (relative) water level.

The sea level trend measured during the satellite altimetry era has strong regional variations (Stammer et al. 2013; Hamlington et al. 2020). There is a growing interest in understanding the factors that affect the estimation of a sea level trend, seasonal and interannual variability at the local scale. This is particularly true near the coast. The latter is difficult to analyze using gridded altimetry products that are based on a smoothing of the order of several tens of kms. Improvements in the processing and availability of coastal altimetry data now allow the analysis of long-term time series based on along-trak data up to 1–4 km from the coast (Marti et al. 2021, Benveniste et al. 2020a, Birol et al. 2021). Differences in the annual and semiannual cycle of sea level have been observed in correspondence with coastal currents and waves trapped on the coast, causing an increase in seasonal amplitude toward the coast (Vinogradov and Ponte 2010, Passaro et al. 2015, 2016). Very local coastal processes can also affect sea level trends very close to the coast, related to waves, currents, atmospheric effects, or freshwater inputs (Woodworth et al. 2019). An initial analysis of nearly 500 altimetry traces spanning nearly two decades of data revealed that 80% of locations do not show significant differences in sea level within the last 15 km of the coast (Benveniste et al. 2020a). While this means that in most cases sea level trends farther from the coast can be extrapolated for coastal risk assessment, significant trend differences have been observed even in highly reliable locations used for decades for sensor calibration (Gouzenes et al. 2020).

2.2 Coastal Currents on the Shelf, Near the Coastline

Ocean currents transport heat, salt, all sort of tracers and floating materials, and are then of crucial importance to regulate climate conditions, at global to local scale. Their monitoring is also a key component in many coastal applications, ranging from biogeochemical resources to marine pollution or search and rescue. During the last two decades, satellite altimetry has played an essential role in the knowledge and monitoring of ocean currents (Fu and Chelton 2001, Stammer and Cazenave 2018). Geostrophic currents can indeed be directly derived from sea surface height altimetry measurements

with respect to the Earth's gravity field (using a geopotential surface—the geoid) and rotation (the Coriolis force).

In contrast to irregularly distributed in-situ data (e.g., hydrographic observations collected by ARGO floats, ships and gliders, surface drifter and moored or ship-based acoustic Doppler velocities) or shore-based HF radars, satellite altimetry provides long time series of spatially and temporally homogeneous information about the circulation and are available at near-global scale. But its use is still limited in coastal areas due to the nearshore data gaps and/or a lower data quality mentioned above. In addition, the spatio-temporal resolution of the original along-track altimetry data is sparse relatively to the scales of many coastal dynamical features. The generation of the most commonly used gridded altimetry current products requires some sort of interpolation which causes smoothing effects and an even coarser spatial resolution. However, as for sea level, because satellite altimetry is a major element of the ocean circulation observing system, several studies have addressed the different issues related to the derivation and exploitation of altimeter-derived coastal current velocities.

Vignudelli et al. (2005) proposed a new data processing strategy to compute altimetric velocities from the Topex/Poseidon (T/P) mission in the Corsica Channel and evaluated their accuracy through a comparison with coincident current measurements from moorings. The conclusion was that an adapted processing improves the data availability and accuracy in a coastal current system. But the corresponding altimetry-derived velocities could only be used at seasonal and longer time scales. In the same area, Bouffard et al. (2008) further improved the data processing proposed by Vignudelli et al. (2005) and used measurements from the four altimetric missions available during the 2002–2005 period in order to increase the spatio-temporal resolution. Data were available at less than 50 km from the coast (between 10 and 49 km) on the continental shelf. They showed that with this multi-satellite configuration, the agreement of altimetry-derived velocities with in situ measurements could be extended to intraseasonal time scales. In this study, multi-mission crossovers were used as virtual current meters to monitor the total surface current component in the study area.

In Salazar-Ceciliano et al. (2018), the flow variability in the eastern shelf of the Gulf of Tehuantepec was documented from intraseasonal to interannual timescales using only the long time series of the T/P+Jason-1+Jason-2 satellite orbit (i.e., a mono-satellite configuration but 20 years of data). Pascual et al. (2015) and Birol and Niño (2015) illustrated the new capability of the Ka-band frequency range SARAL/AltiKa mission (35 GHz, launched in 2013) in terms of coastal current retrieval (up to 7 km from the coast in Pascual et al. 2015). Birol et al. (2021) show that, with the new ESA (European Space Agency) Climate Change Initiative coastal sea level product (Benveniste et al. 2020a), we can estimate the ocean current variability up to 5 km from the coast. Since the work of Vignudelli et al. (2005), we can see how the spatio-temporal extension of the data, the progress made in data processing and in the performance of altimeters allow to better resolve the coastal current variability even closer to the coast on the shelf. Thanks to its further improved observing capability (Vignudelli et al. 2019), the SAR mode of Sentinel-3 (launched in 2016) and of Sentinel 6 (launched in late 2020) will still increase the availability of nearshore altimetry-derived current data.

The synergetic use of altimetry with other types of ocean observations not only allows to validate the coastal altimetry velocity field and estimate its accuracy, but also significantly increases the range of possible applications. Birol et al. (2010) and Jebri et al. (2016) exploited the complementarity between in-situ data, coastal-oriented along-track altimetry products and remote sea surface temperature (SST) observations to improve our knowledge

of the surface circulation scheme in the Mediterranean Sea. Despite the limited spatial resolution of the along-track altimetry data, in these two studies, the picture of the coastal circulation system that is derived appeared fairly coherent at regional scale, and could then be completed by the spatial structures highlighted in the homogeneous and higher resolution SST field.

In Radenac et al (2016), combining altimetry currents with other spaceborne data sets (wind, chlorophyll and SST) along the coast of New Guinea allowed putting scarce in situ hydrographic, biological and/or chemical measurements in a larger scale context. It allowed to identify the major processes involved in the local variability and their period and zone of activity. These studies illustrate how a multi-data combined approach is a unique way to stimulate the use of altimetry in coastal circulation studies (Carret et al. 2019). But we need to keep in mind that in numerous regions, despite the importance of surface boundary currents in local environmental or societal issues, very few or even no in-situ measurements exist. Therefore, it is important to guide the technical and scientific evolution of altimetry toward its operational use within coastal observing systems.

2.3 Ocean and Nearshore Waves

Ocean waves are generally formed by the transfer of energy from atmospheric wind motion to the ocean surface, which becomes a swell wave as time and distance increase. When they reach the nearshore areas, they tend to be unstable and act on coastal changes.

Analysis of these processes on multiple time scales requires the coupling of different data sets provided by in situ measurements and remote sensing techniques. The latter is considered a valuable method to improve the coverage of the measurements and requires some processing and corrections.

Surface winds change the roughness of the sea surface: as the wind speed increases, the sea surface becomes rougher, and consequently the number of specular reflecting faces decreases and also the backscattered power in the nadir direction (Ikeda and Dobson 1995). Using this property, different approaches have been developed to retrieve the surface wind speed from the backscatter coefficients ($\sigma 0$) of radar altimeters, based on empirical relationships as for ENVISAT (Abdalla 2012) or SARAL/AltiKa (Lillibridge et al. 2014), or using neutral arrays (Jiang et al. 2020). Because radar altimeters are nadir-facing sensors, only wind speed can be inferred and not wind direction, unlike scatterometers and SARs. Due to the coarse spatial coverage and temporal resolutions of current radar altimeter missions, radar altimeter data have been used less for surface wind analysis than scatterometer and SAR data, except for the joint analysis between wind and waves, as significant height can also be derived from the radar echo (e.g., Kumar et al. 2013; Young and Vinoth 2013). Archives containing wind speed and wave height data and related quantities for several altimetry missions are now available for easier data exploitation (e.g., Ribal and Young 2019). Recently, altimeter data have been used to document coastal wind fall in Peru–Chile eastern boundary current systems (EBUS) along altimeter tracks (Astudillo et al. 2017) and to improve regional ocean modeling (Astudillo et al. 2019). Coastal data along satellite altimeter tracks have also recently been used to globally quantify the mean attenuation of mean wave height and wave energy flux between the open ocean and the coast (Passaro et al. 2021). Thus, the upcoming NASA/CNES SWOT mission (Fu et al. 2012) will provide new opportunities for studying sea surface winds.

Along the open ocean coasts, nearshore waves (wind waves, rise/run waves, infragravity waves, seiches, …) are a key driver of coastal change and can contribute significantly

to coastal hazards. Wave-induced sea level changes can span time scales from seconds to decades. Swash and runup vary on the resolved time scale of the wave phase, and the wave pattern of the phase mean on the synoptic time scale (Dodet et al. 2019). The magnitude of wave contributions to sea level variations in coastal areas is much larger at very short time scales than at longer time scales. For this reason, waves have mostly been considered in local studies for their substantial contribution to extreme total water levels at open coasts (e.g., Stockdon et al. 2006; Hoeke et al. 2013; Wadey et al. 2017; Pedreros et al. 2018). Global-scale studies of past extreme water levels are often based on tide gauges. Because tide gauges are typically located in wave-sheltered environments, wave contributions to extreme coastal sea levels have mostly not been considered in global-scale coastal risk assessments until recently (as recalled by Wahl et al. 2017). Regional to global scale studies accounting for wave contributions to past (e.g., Ruggiero 2013; Serafin et al. 2019; Rueda et al. 2017; Vousdoukas et al. 2016) and projected coastal water levels are emerging (e.g., Mentaschi et al. 2017; Vousdoukas et al. 2017, 2018a, 2018b; Arns et al. 2017; Vitousek et al. 2017). They highlight the prominent role of wind waves in coastal hazards for low-lying coasts, contributing to coastal erosion and flooding via high total water levels and large energy flows.

Wave patterns may also exhibit low-frequency changes (e.g., Woodworth et al. 2019; Dodet et al. 2019; Ponte et al. 2019; Melet et al. 2016) due to its dependence on many factors that may evolve over long time scales (seasonal to multi-decadal). These factors include (1) changes in geomorphology (e.g., beach orientation, shoreline bathymetry, Familkhalili and Talke 2016; Lentz et al. 2016; Cohn and Ruggiero 2016; Hongo et al. 2018), (2) changes in ocean currents, water depth (including sea level rise), and their interaction with waves (e.g., Hoeke et al. 2015; Arns et al. 2017; Wandres et al. 2017; Quilfen et al. 2018) and (3) changes in deep-water wave characteristics (significant wave height, period, direction) induced by changes in atmospheric circulation patterns and resulting surface winds in response to internal climate variability and climate change (e.g., Morim et al. 2021). Although uncertainties remain regarding the robustness of externally driven trends in wave heights and extremes over recent decades (e.g., Semedo et al. 2011; Charles et al. 2012; Reguero et al. 2019; Young and Ribal 2019; Dodet et al. 2019; Mori et al. 2019), robust changes in wave height, period, and direction are projected for the twenty-first century in several ocean regions (e.g., Hemer et al. 2013; Wang et al. 2014; Morim et al. 2018, 2019, 2021). These low-frequency changes in wave climate are transmitted to total water level changes at the coast through changes in wave patterns and swash. However, few studies have focused on seasonal, interannual, or longer-term changes in wave configuration and swash. In addition to the fact that wave contributions are more important during extreme events, this could also be due to the lack of long and continuous time series of wave configuration and run-up, due to limitations of observations (Dodet et al. 2019; Ponte et al. 2019) and coastal numerical models for realistic representation of coastal morphological evolution (Elsayed and Oumeraci 2017).

One exception is the study by Gainza et al. (2018) in which an interannual time series of wave runup was produced using a meta-modeling approach. A complicating factor in studying low-frequency changes in wave pattern and runup is also their sensitivity to poorly known time-varying local morphology (e.g., O'Grady et al. 2019). Yet, several studies have shown interannual variability in deep-water wave energy flux, shoreline profile, coastline position, and beach width and volume (e.g., Kuriyama et al. 2012; Harley et al. 2017; Norcross et al. 2002; Karunarathna et al. 2016). Recently, Melet et al. (2018) conducted a first-order global estimate of the contribution of wave patterns to past interannual to multidecadal changes in coastal total water levels. Their results highlight the importance

of the wind- and wave-induced contribution to interannual to multidecadal changes in total water levels over the past two decades and suggest that the contribution of waves should not only be considered in studies of extreme events, but also in studies of past and future low-frequency coastal sea level variations and rise (Figs. 1 and 2).

The last type of low frequency nearshore waves is the tsunami waves, long waves with period varying between 1 and 20 min. They are caused by a large and sudden tectonic displacement (wavelength from a few kilometers up to a few hundreds of kilometers) that are generated by sudden tectonic change, usually the result of an earthquake.

Nowadays the satellite altimetry is theoretically useful to detect the relatively small amplitude of tsunami waves in the open ocean by measuring sea surface height. This technique can form also part of a tsunami early warning. It can be also used to compare and validate the forecast models with the aim to improve the propagation of tsunami propagation. For example, the tsunami of 11th March 2011, observed over the Pacific Ocean, has been identified by using three altimetry satellites (Jason-1, Envisat and Jason-2) between 5 and 22 h after the earthquake. Envisat detected the first wave front 5 h and 25 min after
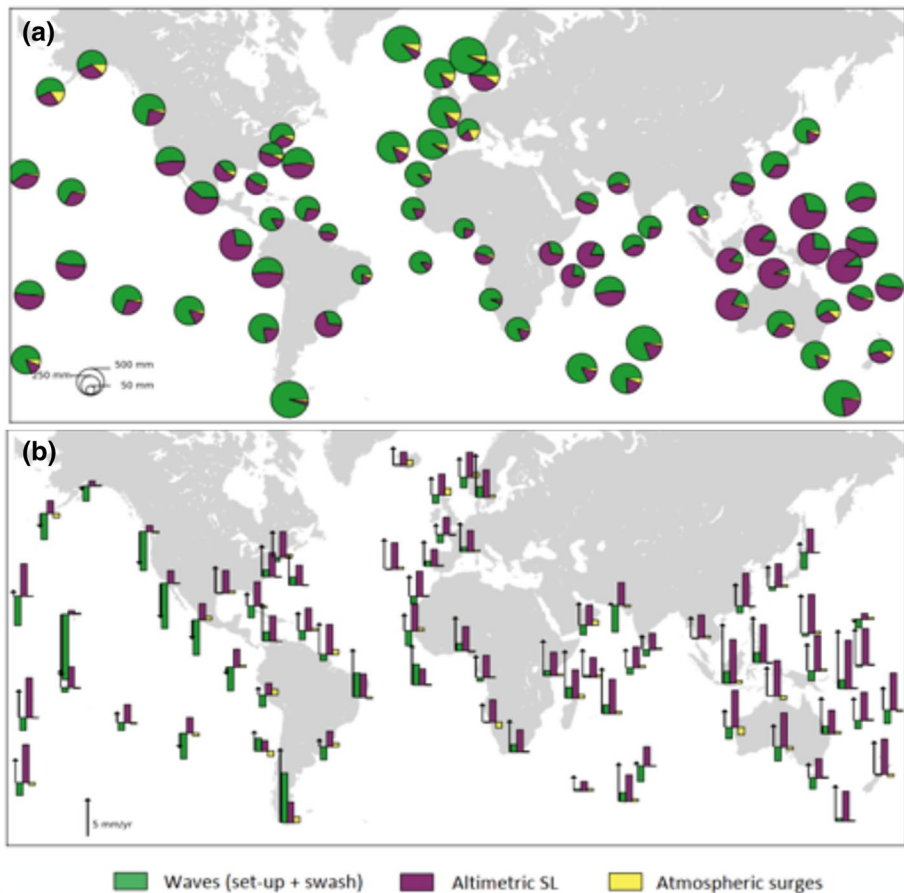

Fig. 1 Coastal sea level decomposed by contributions, waves, regional altimetry and atmospheric surges for the **a** interannual variability and **b** trend (from Melet et al. 2018)
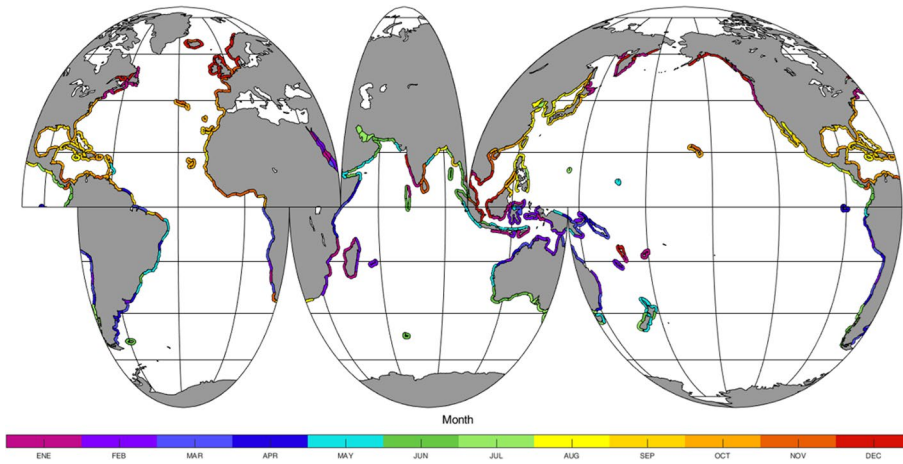
Fig. 2 Coastal map of the monthly distribution of extreme storm surges from satellite data (adapted from Lobeto et al. 2018)

the earthquake with a trough-to-crest amplitude of up to 50 cm. Jason-1 measured a larger amplitude (60 cm), seven and three quarter hours after the earthquake (Godin et al. 2009). Such altimeters are also used for measuring the ocean surface roughness and detecting tsunamis away from the shore. The Jason-1 and TOPEX/Poseidon satellites have been explored by scientists from NASA's Jet Propulsion Laboratory, the National Atmospheric and Oceanic Administration (NOAA), and the French Space Agency (CNES) to detect the tsunami occurred around the Indian Ocean on December 26, 2004, by measuring the crests and troughs of the tsunami as it moved through the Indian Ocean.

2.4 Storm Surges

Flooding risk in coastal areas has been revealed as one of the most relevant impacts to be considered at the present time. Its relevance has increased mainly due to the progressive rise in mean sea level, caused by climate change, and the increase in population density in coastal areas. Sea level rise combined with storm surge contributes to increase chronic flooding occurrences (The term 'surge' refers to a sudden movement of water which is quickly generated but which is soon over (Pugh 1996), while 'storm surge' is usually reserved for higher water level anomalies generated by a severe storm. 'Storm tide' is sometimes used for the description of extreme sea levels and refers to the total observed seawater level during a storm). Such extreme events are already occurring along the eastern coast of north America as well as in many other locations, e.g., in Bangladesh (India) and New Orleans (USA), causing a large number of casualties and economic losses (Sweet and Park 2014; Jacobs et al. 2018; Le Cozannet et al. 2021). The determination of extreme sea levels is therefore a required issue to be able to fully evaluate flooding impacts, which risk is also conditioned by coastal exposure and vulnerability (Toimil et al. 2020).

Apart from the movements in mean sea level and the predicted tide modulations, interactions between the sea surface and the weather atmospheric circulation patterns determine

the total water level on the coastal areas. Surface wind and the atmospheric pressure modify the forces acting on the sea surface.

They trigger setups due to wave nearshore processes, with periods from seconds to minutes, and the storm surge, associated to periods from hour to daily time scale. Physically, the atmosphere forces the storm surge in two ways: (i) changes in atmospheric pressure produce changes in the forces acting vertically on the sea surface, and (ii) forces due to wind stress are generated at and parallel to the sea Surface. The former is called the "inverted barometer response", usually formulated considering a static (isostatic) response of the oceans to atmospheric pressure. Local variations in atmospheric pressure about the mean pressure, in mbar, provide the relation describing that, under an unusual lower atmospheric pressure, the sea level will be higher. Mean sea level atmospheric pressure is usually considered as 1013 mbar; but this value can vary in some regions (e.g., tropical areas usually have lower mean atmospheric pressures). The classical inverse barometer effect approximates sea level changes of ± 1 cm in response to surface air pressure anomalies of $-/+ 1$ mbar. Some processes (for instance baroclinic effects) may however slightly modify this simple inverse barometer relationship, especially in tropical regions (Mathers and WoodWorth 2001). The storm surge generated by the wind is explained by the energy and momentum transfer between the surface atmospheric layer and the sea surface. The surface wind force is defined as the wind stress. The setup of the water level by the wind is proportional to the wind speed, inversely proportional to the water depth and higher when the wind direction is perpendicular to the shoreline and in the case of larger sea surface areas where the wind is blowing. This implies that this wind-induced component can be significant along coasts characterized by shallow continental shelf (Idier et al. 2019). More detailed description about the storm surge response to the atmospheric pressure and wind are provided in Pugh (2004).

Numerous numerical models are available to simulate storm surge. In order to provide long time series, the approach to solve the depth-averaged form of the shallow water equations is often applied. The governing equations are based on the conservation mass and momentum, as described by the Navier–stokes equation. Specific setups are used as function of the model target (e.g., modeling storm surge induced by hurricanes, simulate the nonlinear relation between tide and surge in shallow waters, etc.).

Tide-gauge records are the classical in-situ measurements to analyze sea level variations and extreme values on the coastal area (Woodworth et al. 2016). These instruments measure sea level relative to a local geodetic benchmark, and provide one of the longest records ever measured on oceanographic variables. Records with lengths higher than 100 years are available in different coastal sites worldwide. However, they can be locally influenced by vertical land motions and the stability of the surface they are built upon. Storm surges are usually analyzed from the called 'Non-tidal-residual' (NTR) signal, i.e., the difference between the observed and tide predicted levels. In addition, the 'skew surge' metric (i.e., the difference between the maximum observed sea level and the predicted high tide in a tidal cycle, de Vries et al. 1995) can also provide information about extreme sea levels (e.g., Williams et al. 2016).

Satellite altimeters are a remote data source to analyze sea level that provides regional information (Stammer and Cazenave 2018). The satellite observations are available since the early 1990s and therefore multi-mission data provide three decades of information. Altimeters measure its distance to a referenced surface (e.g., geoid), from which the sea surface height (SSH) can be estimated after a series of range and geophysical corrections (Vignudelli et al. 2011). Range corrections include removing the waves (i.e., sea state bias correction) and tidal and atmospheric sea level variations are included into the geophysical corrections. Sea

level variability is usually analyzed from the Sea Level Anomaly (SLA) data with respect to a mean sea surface, from which the tidal and atmospheric components are removed. Wind and atmospheric pressure effects in the altimeter measurements are usually removed in the altimeter SSH through the Dynamic Atmosphere Correction (DAC, e.g., Carrère and Lyard 2003). Therefore, the analysis of the storm surge from satellite data requires the addition of the DAC to the SLA (Lobeto et al. 2018). Nevertheless, satellite data does not provide time series with a sufficient temporal resolution and gridded products are not suitable for the analysis of extreme sea levels.

Long time series allow the characterization of variations on extreme sea levels, on which the gradual mean sea level rise rides (Menéndez and Woodworth 2010; Lobeto et al. 2021). Spatial seasonal patterns of storm surge are observed throughout the winter season in extratropics, while the monthly occurrence of the storm surges induced by tropical cyclones differs for the affected coastal regions. Main drivers of the interannual to decadal variability can be associated with changes in the climate system but also tidal cycles, such as the of 18.61 years lunar nodal cycle due to the precession of the Moon's orbit around the Earth, can influence extreme water levels (Peng et al. 2019; Haigh et al. 2011). Climate variations can be analyzed by correlating teleconnection patterns with total water levels or directly the climate-related sea level component (storm surge). The North Atlantic Oscillation (NAO) and the El Niño—Southern Oscillation (ENSO), (Muis et al. 2018; Merrifield et al. 1999; Menéndez and Woodworth 2010) are two examples in which natural climate modes trigger higher probability of coastal flooding due to storm surges.

Although many specified locations can be affected by high storm surges, the main world coastal affected by high storm surges are those where severe tropical and extratropical cyclones reach the coast. They are broadly located along the eastern coast of North America, Gulf of Mexico, Northern European coast, Indian coast, East Asia and northern Australia (Fang et al. 2014).

Numerous studies have statistically estimated unusual values of extreme sea levels associated to low probability of occurrence (e.g., 100 year return period). Despite storm surge results from climate variability from monthly to inter-annual scale, return value estimates of storm surge component are more limited. Recent advances in coastal altimetry multimission products and research on statistical extreme analysis to be applied to storm surge data from satellite are therefore a challenge. The studies by Lobeto et al. (2018) and Li et al. (2018) are the first to achieve an in depth analysis of storm surges from satellite data. Lobeto et al. (2018) presented a novel approach based on the application of a non-stationary extreme model to the storm surge monthly maxima from remote data over the North American East Coast. They compared return period storm surge values against similar estimates from tide-gauge data and propose a correction factor. Thus, the results of these studies underlines that the satellite altimetry data show a great potential to study the behavior of sea level extreme events nearshore where in situ information is not available.

3 Shoreline (Water/Sediment Contact): Survey and Vulnerability

The knowledge of trends and variability in the shoreline position is useful for policy making to design coastal zone monitoring and human interventions, but also to scientists to better understand and predict the shoreline dynamics. By definition, the shoreline is located at the intersection of water and land surfaces. However, this intersection is dynamic, such that there is not a single shoreline indicator, but a range of possible shoreline indicators,

depending on the nature of the data and the objective. According to Boak and Turner (2005), these proxies are generally of two types: either a feature that is visible in coastal imagery (e.g., instantaneous waterline, vegetation line) or the intersection of a tidal datum with the coastal profile (e.g., mean high water). Another category emerged these last 2 decades, based on the application of image processing techniques to extract proxy shoreline features from digital coastal images that are not necessarily visible (e.g., time-averaged waterline derived from a high-frequency image dataset, as in Aarninkhof et al. 2003). Optical satellite images appear logically as a source of shoreline data, while synthetic aperture radar (SAR) imagery allows observing the Earth even in the night or cloudy conditions. Triggered by the increase of spatio-temporal resolution of satellite images since the 80's, but also of the amount of publicly available satellite images, significant progresses have been done in the production of satellite-derived shoreline, opening a new era for shoreline evolution/change studies.

3.1 Satellite Derived Shoreline

Shoreline detection methods rely mainly on the analysis of near-infrared (NIR) spectrum, as it is absorbed by water and gets reflected by vegetation and dry soil (Work and Gilmer 1976). The methods based on NIR use either this sole band (e.g., Rundquist et al. 1987) or indices developed from the conjunction of other bands. The most widely used indices are the normalized difference vegetation index (NDVI) which enhances the water feature with red band (e.g., Tucker and Sellers 1986), the normalized difference water index (NDWI) which uses the green band (e.g., McFeeters 1996), and the modified normalized difference index (MNDWI) which uses the short-wave infrared (SWIR) to overcome noise issue (Vos et al. 2019a, b). The main steps are generally: (1) pre-processing (noise reduction and image correction, as, e.g., radiometric and geometric corrections; ortho-rectification), (2) land-sea segmentation (i.e., the algorithm allowing to separate the land from the sea, for instance by edge detection, classification or band thresholding methods), (3) post-processing (as e.g., "water level correction"). For step (2), several approaches have been proposed such as edge detection, segmentation and classification approaches (Toure et al. 2019).

The spatio-temporal resolution is a key issue for shoreline survey. With the time, the pixel size of publicly available optical image has decreased from 80 m for the first Landsat missions 1–3 (1972–1983), to 30 m for Landsat 4–8 (1982—present) and 10 m for Sentinel-2 (2015—present). At the same time, the satellite revisit period has decreased from every 18 days for Landsat 1–3, to 16 days for Landsat 4–8 and 5 days for Sentinel-2. In addition, high resolution imagery can be used, as for instances the Pleiades images (0.5 m resolution and revisit period of few days) provided by CNES (Centre National d'Etudes Spatiales), IKONOS, Quickbird, or other private initiatives based on nano-satellites (e.g., SkySat, with a metric resolution and daily revisit period). A semi-automatic method to extract a shoreline from commercial Earth observation satellite (IKONOS) images, based on mean shift segmentation and the identification of water bodies including the shoreline refinement, has been presented by Li et al. (2003). The Quickbird multispectral images have been used by Giannini and Parente (2015) to extract the coastline by segmentation from the multispectral bands. The drawback of such missions is that they are not all publicly available.

A few years ago, Google launched the Earth Engine platform (GEE). This consists of a multi-petabyte analysis-ready data catalog co-located with a high-performance parallel

computation service, and allows reducing image processing time to only a few minutes per image (Gorelick et al. 2017). This platform triggers the use of a full collection of satellite images and of state-of-the-art image processing techniques. In 2018, this led to the first global scale assessments of shoreline evolution (trends) on sandy beaches, from 1984 to 2015 and 2016, respectively (Mentaschi et al. 2018; Luijendijk et al. 2018). However, these studies focused mainly on trends, while the method they use exhibit some limits, especially out of micro tidal areas. Vos et al. (2019a) made the first deep investigation on capability to detect various time scales of shoreline changes from satellite images, including tidal corrections.

Historically, shorelines were detected based on the use of single images and indexes thresholds. To tackle the global scale, methods based on composite images have been developed (Mentaschi et al. 2018; Luijendijk et al. 2018). For instance, Luijendijk et al. (2018) relied on NDWI and cloud free global annual composite images. More recently, a promising approach has been developed based on the extraction of sub-pixel resolution, the use of single images, an image classification method allowing to better identify the breaking areas as water areas, and tidal corrections. This method is implemented in the publicly available CoastSat Python toolkit (Vos et al. 2019b). As an illustration of the method skills, on the Narrabeen site (Australia), on the same input dataset, the RMSE equals 8.2 m, 9.5 m and 13.7 m, in Vos et al. (2019a), Liu et al. (2017) and Luijendijk et al. (2018). After Vos et al. (2019a), the first improvement is due to the use of the refined four-class pixel classification, while the second improvement is due to the use of single image rather than image composites, plus the application of pansharpening (i.e., increase the spatial resolution of the multispectral bands by using the higher spatial resolution panchromatic band, see, e.g., Liu et al. 2017), a downsampling and tidal correction. Moreover, Castelle et al. (2021) investigated the uncertainties associated with satellite-derived time series of shoreline position on a high-energy meso-macrotidal beach. They proposed a new total water level threshold accounting for wave runup which, combined with a horizontal correction of shoreline position based on average beach slope estimated from in situ data, halves shoreline error and doubles the number of usable satellite images, thus dramatically improving shoreline reconstruction along such coasts.

On the other hand, SAR imagers can be used and present the advantages of penetrating the cloud cover and allowing nighttime acquisitions. SAR images really started to be used for shoreline detection in the 90's (see e.g., Lee and Jurkevich (1990), which proposed a technique based on the Sobel-Feldman edge detection algorithm for a small portion of a SEASAT image). Contrary to optical images, the analysis of SAR images encounters the difficulty in discriminating wet and dry sand, which is a key issue especially in meso to mega-tidal areas. Today satellites such as TerraSAR-X can provide SAR images with a 3 m resolution, with a revisit period of 11 days. As an example of shoreline detection using such SAR images, Vandebroek et al. (2017) derived shoreline on a "mega-scale" beach nourishment project in the Netherlands, called Sand Motor (De Schipper et al. 2016). The horizontal accuracy of the derived shorelines was approximately 50 m, which was sufficient to assess the larger scale shoreline dynamics of the Sand Motor. Thus using SAR image as TerraSAR-X appears as a valid option for assessing temporal shoreline changes of the order of tens of meters at approximately monthly intervals. It should also be noted that many developments have been done to build Digital Elevation Models (DEM) on emerged or intertidal areas using satellite measurements (for a review, see Salameh et al. (2019) and Sect. 3).

There are many perspectives of improvement in the way shorelines are derived from satellite images. One relates with the necessity, for practical applications, to project an

instantaneous shoreline to a reference elevation. Indeed, DEM- and shoreline-oriented method rely both on using nearby water level measurements or hydrodynamic models, assuming that the altitude of the waterline equals this data. One promising way to tackle the runup issue is to use video streams from satellite. This would allow computing time-averaged images to remove much of the influence of wave runup on mapped shoreline positions, as it is done since many years when using terrestrial video-monitoring systems providing oblique images (e.g., Aarninkhof et al. 2003). Finally, the increase of the amount of free satellite images, together with platform easing their use and the increase of open access processing tools, should lead to a much larger use of these images for shoreline evolution studies and significant developments in the coming years/decade, to tackle intra-annual to pluri-decadal scales and local to global scales.

Moreover, the machine/deep learning techniques open new strong perspectives to map waterlines and coastal features from the satellite. Zhang et al. (2013) have investigated the shoreline evolution by the use of support vector machine (SVM) classification algorithm. They have optimized different SVM kernel functions (Polynomial, Radial basis and Sigmoid) and used the Sigmoid kernel function which outperforms other functions. The water-index-based method has been compared to the SVM algorithm by Choung and Jo (2017) for plotting accurate shorelines using high-resolution satellite images; they have highlighted that both techniques accurately identified coastal zones with the SVM outperformed the water–index for coastal ones with irregular shapes and shaded areas.

3.2 Coastal Vulnerability from the Shoreline Change

Past studies focused on the shoreline change and prediction, including empirical analysis of beach stability (Wright and Pilkey 1989; Basco 1991), analysis of natural and anthropogenic beach loss and gain, identification of relative changes among coastal units (Siddiqui and Maajid 2004), shoreline response to energy driven forces (Fenster et al. 1993).

Joevivek et al. (2013) analyzed the coastal vulnerability in Southern India using a remote sensing approach of Landsat sensors (Multispectral Scanner (MSS), Thematic Mapper ™ and Enhanced Thematic Mapper Plus (ETM+)). They classified the vulnerable risk zones on the basis of the shoreline change and the coastal vulnerability index (CVI) which include six vulnerable parameters, namely coastal morphology, shoreline change rate, coastal slope, relative sea level change, mean wave height and mean tide range. The accurate identification of the first three vulnerable parameters from satellite products have been reviewed in several works (e.g., Bishop-Taylor et al. 2019; Vos et al. 2020). For example, the beach face-slope has been evaluated along eight diverse sandy/gravel beaches by Vos et al. (2020) from satellite-derived shorelines coupled with tidal models to create intertidal digital elevation models (Bishop-Taylor et al. 2019; Tseng et al. 2017).

Gomez et al. (2014) characterized the coastal vulnerability in the Outer Hebrides, Scotland, using Landsat imagery. They have provided some insights into vulnerable areas in particular; their study supports flooding and erosion from a series of change patterns of coastal environments over the period 1989–2011 considering the recent shift of the coastlines and the land-based vegetation which are assessed by the Digital Shoreline Analysis System (DSAS). Several researchers investigated the extraction of satellite image features related to coastal vulnerability. A software of digital shoreline analysis (DSAS) has been developed to calculate the annual rate of beach changes in the north-west of Nile Delta, from Landsat data, and detect pre and post-beach responses to highly energetic conditions and coastal protection structures (Dewidar and Frihy 2007). The temporal coastline

changes between 1986 and 2001 and the associated sediment characteristics have been analyzed by El Banna and Hereher (2009) from Landsat images for the Mediterranean coast of northern Sinai.

Elnabwy et al. (2020) investigated the shoreline changes in the northeast of Nile Delta, Egypt, exposed to a series of natural and anthropogenic forcing factors with the aim of supporting the integrated coastal management. They developed a novel method to assess the shoreline changes based on the combination of SVM classification for Landsat images and GIS for improving the accuracy of shoreline estimation.

The deltas provide good examples of studies performed at the global scale from measuring different physical quantities by Earth Observation satellite data, such as near-infrared images, optical remote sensing, etc. Syvitski et al. (2009) used visible and near-infrared images from the Moderate Resolution Imaging Spectroradiometer (MODIS) satellite, together with in-situ observations, to determine whether delta plains are keeping up with rising sea levels (33 world's largest deltas considered). They estimated that the delta surface area vulnerable to flooding could increase by 50% under the projected sea-level rise over the twenty-first century. This work was updated, and completed, by Tessler et al. (2016) using optical remote sensing (Landsat) to map vegetation patterns and the locations of upstream river bifurcations, combined to environmental indicators. They developed an anthropogenic change typology in 48 global deltas. By identifying quantitatively similar deltas, they make their scientific results transferrable to other deltas. More recently, Besset et al. (2019) analyzed over a 30 year time span shoreline mobility and area change of 54 world's deltas from a heterogeneous satellite image database (Landsat and SPOT5/6). They showed that more than half of the deltas are in overall erosion. They argued that the dams currently in place will reduce sediment load of half of the deltas by more than 50% and by 100% for 15 of them.

4 Reconstruction of the Topography and Bathymetry: Digital Elevation Models

Only a small fraction of world coasts is surveyed by hydrographic and geographic national services, and nautical charts and DEMs are decades old. This leads to severe uncertainty in the risk assessment and forecast of storms and climate changes impact (Benveniste et al. 2020b; Melet et al. 2020). Characterization of physical properties of the coastal zone is thus needed for coastal hazard assessments. In this section we focus on retrieving the topography and bathymetry continuum of coastal areas (coastal land and intertidal flats topography and sea coastal bathymetry) using optical and SAR observations.

4.1 Coastal Land Topography

Satellite remote sensing techniques now offer a good alternative for DEM construction over large spatial areas with sufficient resolution (< 100 m): global DEMs such as the 90 m resolution Shuttle Radar Topography Mission (SRTM) (Farr et al. 2007) (widely used for broad scale flood modeling, e.g., Ettritch et al. 2018; Neumann et al. 2015; Kulp and Strauss 2018), commercial 5-m ALOS AW3D30 (JAXA, Tadono et al. 2016) and 8 m resolution WorldDEM (Airbus, on-demand). However, they are often years old and do not reflect the rapid evolution of dynamic coastal areas. By analyzing stereoscopic pairs of satellite optical images (Tateishi and Akutsu 1992), it is possible to study large coastal areas

with vertical errors of less than 0.5 m. Examples using Pleiades are given in Collin et al. (2018), Almeida et al. (2019) (Fig. 3) and Taveneau et al. (2021).

4.2 Intertidal Flats Topography

Intertidal environments are gently sloped surfaces lying as a buffer zone between land and sea. They are perpetually evolving coastal landforms which are primarily located in tide-dominated environments and sheltered coastal embayments (Gao 2019; Klein 1985). Likewise other coastal features, intertidal flats provide essential services. They are a reservoir for biodiversity providing, for instance, habitat for large communities of migratory shorebirds (Agardy and Alder 2005), support millions of people worldwide, stabilize the coastline, protect from storm surges, and offer protection against coastal flooding (Murray et al. 2019). Intertidal flats are currently supporting the pressure of both anthropogenic activities and climate change related stressors. Between 1984 and 2016, a 16% decrease of worldwide intertidal surfaces has been documented by Murray et al. (2019). For a better understanding of intertidal environments, there is nowadays an increasing need and demand for regular and updated information related to their topography. Such frequent revisit monitoring can be provided by spaceborne sensors.

Monitoring intertidal topography and generating intertidal DEMs is mainly achieved using the waterline method introduced by Mason et al. (1995). The waterline (shoreline) is the instantaneous water/sediment interface (cf. Sect. 2). The method uses a series of waterlines extracted from satellite images (optical and radar) sampling the different tidal stages. Then, an altitude is assigned to each waterline, using SSH either measured by tide gauges or extracted from hydrodynamic models at the exact time of the image acquisition (Fig. 4a). The leveled waterlines are finally assembled (Fig. 4b) and interpolated to form a gridded DEM (Fig. 4c). The main approximation of this method is to consider the intertidal topography as static under the assumption of no change occurring during the acquisition period of the images (Mason et al. 1995; Ryu et al. 2008). Therefore, it is crucial to keep the acquisition period as short as possible and to determine the optimal combination
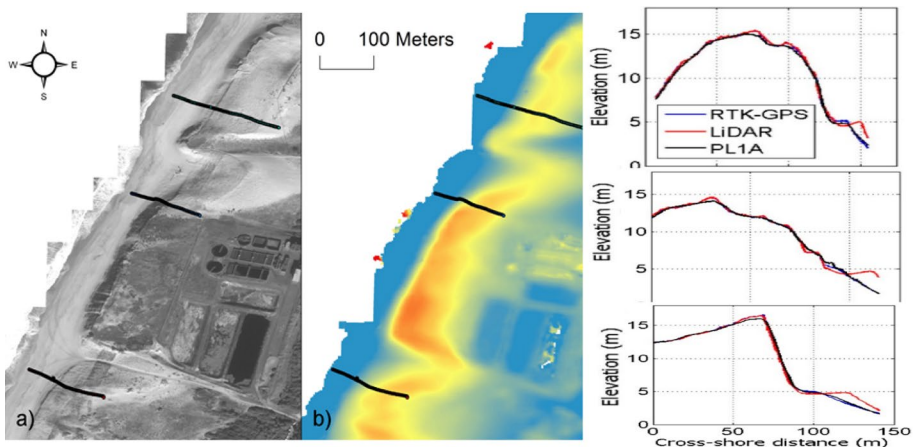

Fig. 3 **a** Orthophoto and **b** Digital Surface Model from Pleiades stereo pair showing the locations of the transects for comparison between the RTK-GPS, Pleiades (PL1A) and LiDAR data shown in the lower panels (from Almeida et al. 2019)

between the acquisition period and a complete sampling of the tidal cycle. It is also recommended to use images acquired at extended calm periods depending on the study site in order to avoid, to a maximum, any possible topography changes during the acquisition period (Li et al. 2014; Salameh et al. 2020).

Historically, it was difficult to reduce this period below a couple of years due to the scarcity of images. Nowadays, owing to the deployment of Sentinel-1 and Sentinel-2 missions, short acquisition periods (~3 months) are more easily achievable. The quality of the generated DEMs depends on an adequate sampling of the tidal cycle in order to cover all the intertidal area by leveled waterlines, but it also depends on the planimetric precision of the position of the extracted waterlines and the vertical precision of the sea level information used whether it was based on tide gauges or ocean circulation model outputs (Heygster et al. 2009; Kang et al. 2017; Salameh et al. 2020). More precisely, the accuracy is governed by the following factors: (i) the planimetric resolution of the sensor, (ii) the geometric corrections, (iii) the horizontal accuracy of the edge detection (waterline extraction) technique, (iv) the intertidal topography slope, (v) the surface water slope, and (vi) the accuracy of sea level information (see Salameh et al. 2020 for a detailed description). The latter factors affecting the accuracy are sensor- and site-dependent which complicates the ability to assess the performance of the method. However, relatively accurate DEMs were generated using this method in various geographic regions where accuracies of about 20 cm were obtained (which is the case of the Arcachon intertidal DEM shown in Fig. 4).

The waterline method was applied to various study areas across the globe using a variety of sensors. Different techniques were used to extract waterlines, to level waterlines and to interpolate them. The common approach between the different studies is the reliance on manual processing at some point during the processing of images or the post-processing of waterlines. First attempts to automatize the waterline method were performed by Heygster
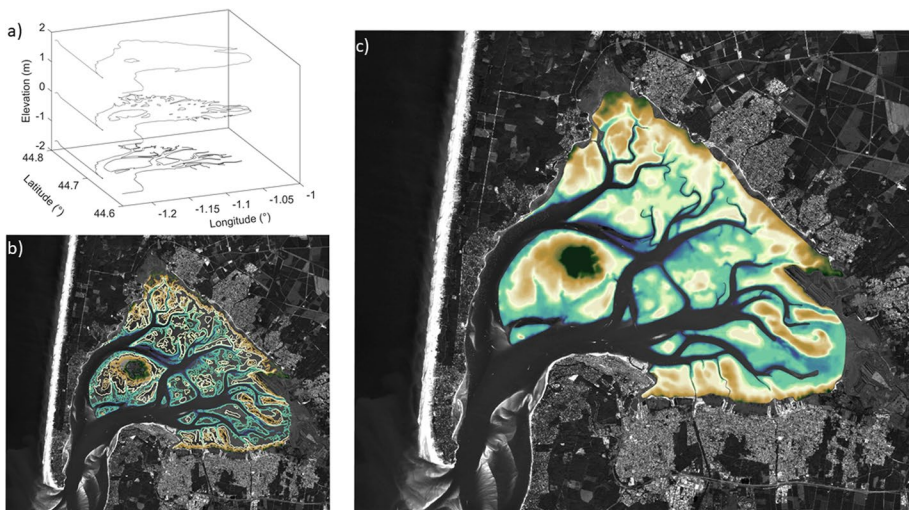

Fig. 4 The waterline method results obtained by Salameh et al. (2020) for the intertidal area of the Arcachon Bay using Sentinel-1 and Sentinel-2 images. **a** Examples of three leveled waterlines extracted from Sentinel-1 (or/and Sentinel-2) images which were acquired at high, intermediate, and low tides; **b** Assembled waterlines for an observation period of 4 months (between the first of June 2018 and the end of September 2018); **c** the waterline-derived DEM obtained after interpolating the waterlines using the kriging method

et al. (2009). In Salameh et al. (2020), a quasi-automatic procedure was developed to use the method automatically with an ability to process radar and optical images without needed adaptations for each type of images. Rendering the method fully automatic is a crucial task in order to make it available for operational use and for large scale intertidal monitoring.

Another method used for generating intertidal DEMs is Interferometric SAR (InSAR). This method is a well-known established technique for inland topography monitoring but proven also reliable for intertidal environments (Choi and Kim 2018; Lee and Ryu 2017; Won et al. 2003). It uses two or more complex-valued (real and imaginary parts as the in-phase- I - and quadrature- Q - components) SAR images (known as master and slave images) acquired from different perspectives in order to generate a three-dimensional model from the images phase difference (Hanssen 2001). The InSAR method has a great potential to generate high-quality DEMs but depends as well on various criteria and conditions (Bamler and Hartl 1998). Interferometric coherence is an essential parameter that reflects the quality of an interferogram, the similarity between the master and slave images, and thus the ability to generate accurate DEMs. Many decorrelation factors (volumetric, signal to noise, temporal, and geometric decorrelations) reduce the magnitude of the coherence (Hanssen 2001). A major limiting factor for intertidal areas is the temporal decorrelation resulting from physical changes (changes in surface water and surface roughness, remnant water, etc.) in the scene between the master and slave images. Thus, a short temporal baseline (time difference between two acquisitions) is required for generating accurate DEMs. Therefore, single-pass interferometry with two antennas on the same platform acquiring images at the same time is recommended for intertidal areas over multi-pass interferometry systems.

Radar altimetry recently demonstrated a good capability to directly estimate along-track elevation profiles of the intertidal areas (Salameh et al. 2018). Benefiting of the non-penetration of the electromagnetic wave in the medium (sand or mud) in wet environments, high accuracy elevation profiles were obtained from data collected by Cryosat-2 at Ku-band (~ 13.6 GHz) using the SAR technique or by SARAL at Ka-band (35.5 GHz) using the Low-Resolution Mode (LRM) technique. Satellites on long period repeat orbit or on drifting orbit offer the opportunity to more densely sample intertidal flats. Accurate retrievals can also be expected from the recently launched lidar altimetry missions (e.g., ICESat-2 (Markus et al. 2017) and Global Ecosystem Dynamics Investigation Lidar—GEDI (Hancock et al. 2019)). Intertidal topography is likely to benefit from the SWOT mission, to be launched end 2022, the first altimeter to estimate elevation in two swaths owing to the near-nadir SAR interferometry technique (Biancamaria et al. 2016). A recent study analyzes the potential of this technique for generating DEM of intertidal flats based on simulation (Salameh et al. 2021).

Mapping the topography of intertidal systems using spaceborne sensors in a regular manner provide useful and needed information for accurate hydrodynamic modeling, and opens the way for monitoring topographic changes and estimating sediment budgets. By using the waterline method, Salameh et al. (2020) estimated the sediment budget between 2016 and 2018 for the Arcachon Bay and the Bay of Veys located both on the Atlantic façade of the French coast where both bays showed net volume losses of 1.12×10^6 m^3 and 0.70×10^6 m^3, respectively, over the study period.

4.3 Coastal Sea Bathymetry

In the coastal zone, optical satellite-derived bathymetry (SDB) can reach much finer resolution thanks to two approaches (Pleskachevsky et al. 2011): modeling of radiative transfer of light in water for the processing of optical images, and methods based on the influence of topography on waves. Each method/sensor comes with its own strengths, limitations, and scope of applications (Gao 2009; Jawak et al. 2015). Specifically, methods based on the radiative transfer perform better in clear and calm waters, whereas techniques based on water depth inversion require waves and more turbid waters.

The pioneering technique using aerial multispectral photographs (Lyzenga 1978) was expanded to multi-spectral optical satellite images with first attempts made using Landsat data, followed by wider applications to other satellites such as Sentinel-2 (Caballero and Stumpf 2019; Evagorou et al. 2019; Sagawa et al. 2019). SDB is calculated based on the attenuation of radiance as a function of depth and wavelength in the water column, using analytical or empirical imaging methods. Bathymetry can be estimated down to depths from a few meters (e.g., northern Baltic Sea) to 20–30 m (e.g., Mediterranean Sea) depending on the maximum penetration depth of sunlight, which varies with season, location, turbidity, bottom reflectance, etc. The spatial resolution of such bathymetry depends on the optical sensor, from coarse resolution with for instance Landsat (~30 m resolution), to medium resolution with SPOT and Sentinel-2 (10 m, Fig. 5) and to high resolution (sub-metric) with commercial satellites such as WorldView (Monteys et al. 2015). The accuracy of this method is lower than with lidars or echo-sounders, but is a cost-effective solution to map the nearshore bathymetry over large areas.

Other techniques for estimating bathymetry from optical images use wave kinematics (Abileah 2006; Danilo and Binet 2013; Poupardin et al. 2015). This allows depths of up to 40–60 m to be resolved (Bergsma and Almar 2020). Bathymetric inversion codes developed from wave dispersion relationship make use of the temporal information contained
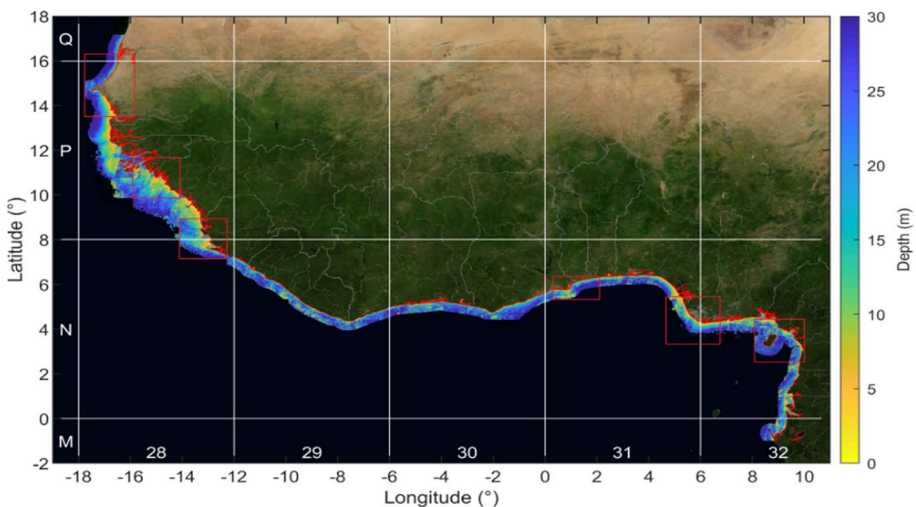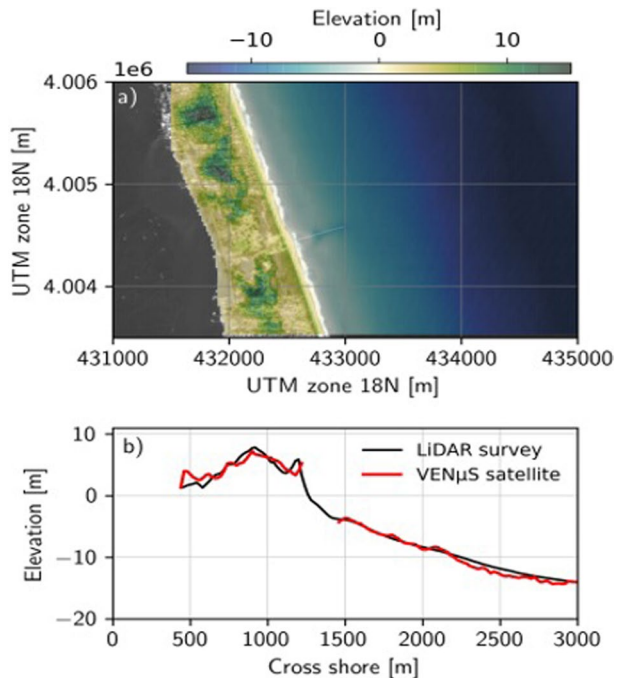

Fig. 5 S2Shores (Satellite to Shores) bathymetry composites for the West Africa Region from Daly et al. (2022). Background image is MODIS Blue Marble, NASA Earth Observatory. Red boxes outline the area of the six hot-spots studied in Daly et al. (2022)

in the spatial images and were applied to different satellite observations: IKONOS (Abileah 2006), WorldView-2 (Mc Carthy 2010), SPOT5/6 (Poupardin et al. 2015), Sentinel-2 (Bergsma et al. 2019; Daly et al. 2022) and Pleiades (Danilo and Binet 2013; Almar et al. 2019) for unprecedented accuracy when applied at regional scale (correlation of 0.8 and RMSE = 1.4 m between the estimated bathymetry from Pleiades data and in-situ bathymetry measurements in the example of the Cap Breton in France; Almar et al. 2019).

4.4 Continuum Land Sea Digital Surface Models (DSM)

Bathymetry and topography can be combined in the same vertical reference to generate a continuum land sea DSM (Bergsma et al. 2021). This is clearly the way forward for coastal studies to document exchanges of sediment between the lower and upper shoreface (Anthony and Aagaard 2020) and flooding numerical simulations, e.g., Muis et al. 2020). Several recent studies made use of deep learning approaches (Sagawa et al. 2019) that brings great expectations to solve satellite-based bathymetry issues of complex physics and environments and computational costs (Danilo and Melgani 2019; Al Najar et al. 2021). Coastal morphology changes over a wide range of timescales (from storm events, seasonal and interannual variability to longer-term adaptation to changing environmental conditions), in particular in response to changing incoming wave regimes (e.g., Karunarathna et al. 2016; Bergsma et al. 2019, Fig. 6) and human interventions. Despite its high potential, SDB has only been applied to limited space areas, and efforts remain to be done to map nearshore bathymetry and its time-evolution at global scale (e.g., Mayer et al. 2018; Wölfl et al. 2019; Benveniste et al. 2019).

Fig. 6 VENµS satellite mission showing the barrier island at Duck, North Carolina, USA, and a comparison of the land-sea coastal morphological continuum with ground measurements along a cross-shore profile (From Bergsma et al. 2021)

5 Coastal Vertical Land Motion

The vertical land motion (VLM), i.e., subsidence or uplift of the land surface, is a complex spatio-temporal process that can be of natural origin, as driven by glacial or sedimentary isostatic adjustment, land water storage, tectonics, volcanism, sediment compaction, or/ and of human-induced origin as withdrawal of groundwater, oil and gas extraction, specific land usage and building upstream dams impacting sediment transport by rivers (Shirzaei et al. 2021). Although VLM measurements remain a challenging issue, the advances in satellite-based techniques, such as InSAR, GNSS (Global Navigation Satellite System (Santamaría-Gómez et al. 2017), and satellite altimetry combining with tide gauges (Wöppelmann and Marcos 2016), allow to measure VLMs at local to regional scales.

The GNSS solutions, free and publicly available, based on a global network of stations are provided by different centers: the Nevada Geodetic Laboratory (NGL, http://geodesy.unr.edu/), the Jet Propulsion Laboratory (JPL, https://sideshow.jpl.nasa.gov/) the German Research Centre for Geosciences (GFZ, https://www.gfz-potsdam.de/) and the University of La Rochelle (ULR SONEL, http://www.sonel.org/) among others. We note here that the French SONEL data centre provides the local rate estimates and associated uncertainties for the vertical positioning component for worldwide stations in a comprehensive framework (maps, time series and tables, co-located tide-gauge station).

As an example of GNSS solutions application in the Southwest and Central Pacific region, where inhabitants of low-elevation islands are particularly vulnerable to sea level rise, Ballu et al. (2019) proposed a complete re-analysis of the VLM rates obtained from the GNSS solutions, considering the geodynamic context of each site. They observed significant VLM variations ranging from 1.6 ± 0.3 mm/year (uplift) to -5.4 ± 0.3 mm/year (subsidence) over 2002–2017. They not only provided VLM rates and associated uncertainties, but also very useful criteria for forecasting future coastal sea levels based on the geodynamic context.

A second manner to obtain VLM rates is by differencing satellite altimetry-based SSH and tide gauge measurements. While satellite altimetry provides absolute (geocentric) sea level, tide gauges measure relative sea level because they cannot distinguish between ground VLM and absolute sea level change. Several studies using this methodology, sometimes combined with GNSS measurements, were conducted at global (Ostanciaux et al. 2012; Pfeffer and Allemand 2016; Santamaría-Gómez et al. 2014; Wöppelmann and Marcos 2016) and regional scale (Fenoglio-Marc 2002; Fenoglio-Marc et al. 2012; Kuo et al. 2004; Letetrel et al. 2015, among others).

At regional scale, along many low-lying coastlines in the world, human-induced land subsidence occurs at a faster rate than the climate-induced sea level rise, increasing the vulnerability of population to coastal flooding (Allison et al. 2016; Becker et al. 2019). This is the case, for example, in Manila (Philippines) where Raucoules et al. (2013) demonstrated, from InSAR (from ERS and Envisat images), that the city of Manila was locally affected by vertical ground motions of about 150 mm/year from 1993 to 2010. This subsidence has been in part linked to the increase in groundwater pumping (Rodolfo and Siringan 2006). The megacity of Jakarta (Indonesia) is also subject to subsidence mainly driven by excessive groundwater extraction. Combining leveling surveys, GNSS observations, and InSAR (ALOS-PALSAR) analysis, the subsidence rate there is estimated in the range of 30–100 mm/year during 1974–2010 (Abidin et al. 2015; Chaussard et al. 2013).

In large deltas it is difficult and costly to quantify the VLM from ground-based surveying techniques. However, the VLM is a key part of their future survival and several

studies showed that most major river deltas are now sinking (Ericson et al. 2006; Syvit-ski et al. 2009). For example, in the Ganges–Brahmaputra delta, (Becker et al. 2020) esti-mated regional long-term land subsidence rates between 1 and 7 mm/year since 1990s, by combining river and tide gauge records with ocean satellite altimetry measurements. They showed that in some regions of the Ganges–Brahmaputra delta, relative sea level could rise up to 140 cm by 2100, almost twice as high as previously projected (IPCC 2014), mostly a result of land subsidence. In Vietnam's Mekong delta, by analyzing 78 ALOS PALSAR InSAR interferograms, Erban et al. (2014) estimated regional subsidence rates, mainly due to groundwater pumping, are in the range 10–40 mm/year during 2006–2010. Minderhoud et al. (2018) extended this dataset (Landsat 8) and analyzed the link between land-use change and subsidence rates. Agricultural areas and cities experienced the high-est subsidence rates (18–20 mm/year). If the groundwater extraction continues to increase, the induced subsidence could drown the Mekong delta before the end of the century (Min-derhoud et al. 2020). In the Egypt's Nile Delta, Rateb and Abotalib (2020) revisited the subsidence patterns using InSAR Sentinel-1 and GNSS data over 2015–2019. They high-lighted a recent predominant anthropogenic control on land deformation, in particular along the coastal margins where the subsidence (3–8 mm/year) is due to sediment natural compaction and exacerbated by the Nile river flow sediment decrease due to building of dams.

Although the subsidence affects sea level local rates, assessments of its coastal impacts are still lacking on a global scale (Nicholls et al. 2021). Earth observation from space rep-resents a powerful tool, with unprecedented spatial and temporal resolution, to answer this major challenge.

6 Bio-physical Characteristics of Sediments and Suspended Sediment

In coastal systems such as estuaries and deltas quantifying both sedimentary and sus-pended particulate matter (SPM) budgets are important regarding coastal management, navigation ability, erosion/accumulation of sediments, transport of pollutants, fisheries pro-ductivity, and drinking water resource, as well as preservation of the biodiversity of coastal and marine habitats. Several coastal zones and related ecosystems disappear due to various causes such as, sea level rise, increased storm frequency, etc. However, such an informa-tion is either missing or is not accurate enough due to the sampling difficulties, especially in mudflat domains. In response to these major challenges, optical imaging is increasingly used for mapping coastal sediment deposits at low tide as well as SPM flow at high tide. It provides a synoptic overview of bio-physical characteristics of sediments over estuarine and deltas systems.

6.1 Bio-physical Characteristics of Sediment

The use of optical imaging including multispectral and hyperspectral systems with in situ measurements is well suited for improving our understanding of the sediment dynamics in response to physical forcing or biological mechanisms (Verpoorter et al. 2020). However, interactions between sediment and biology compartments under hydrodynamic forcing remain very complex (Stal 2010). However, remotely sensed products derived from spec-tral, analytical or radiative models (Combe et al. 2005; Verpoorter et al. 2014; Launeau et al. 2018) can provide relevant information on bio-physical properties (Fig. 7), improving

our knowledge about mechanisms and dynamics between compartments. Sediment erodibility is mostly controlled by tidal currents, waves, and sediment dehydration during air exposure. Tidal currents are responsible for sediment transport and therefore of the sediment supply in estuaries while waves are responsible about deposition or erosion of the sediment. Sediment erodibility/stability depends on abiotic effects including moisture content (Fig. 7c), grain-size distribution, roughness, compaction, as well as biotic effects including microphytobenthos developments (Fig. 7d, e), over sediment surfaces generating a protective biofilm called EPS (extracellular polymeric substance). Riethmüller et al. (2000) investigated the bio-stabilization phenomenon throughout the microphytobenthos mapping (Fig. 7d). Conversely, other biological factors such as grazing and feeding determine bio-destabilization processes (Adam et al. 2011). On the other hand, it is important to discern cohesive from non-cohesive material (Fig. 7) as a starting point of erodibility assessment (critical shear stress calculation) and then transport from grain-size trend (Menuge et al. 2020). Grain-size distributions and water content are spatially highly correlated. This is because coarser sediments are drier than silty sediments due to the higher efficiency in the percolation process.

Multispectral sensors have been also used to identify the land cover types and classify the distribution of the vegetation density and the sediment characteristics from the spectral response of the systems. Classification approaches have been performed using both segmented images as well as NDVI maps for an accurate discrimination between water and non-water systems (sand, gravel, vegetation, etc.). Such approaches, including supervised and unsupervised classification, have different levels and options for the accuracy and the rigidity of classification depending on the different physical factors, considered in the implementation of the methods. Coastal linear features have been identified with very high spatial resolution by Pardo-Pascual et al. (2012) with the aim to support long-term monitoring of time changing patterns.
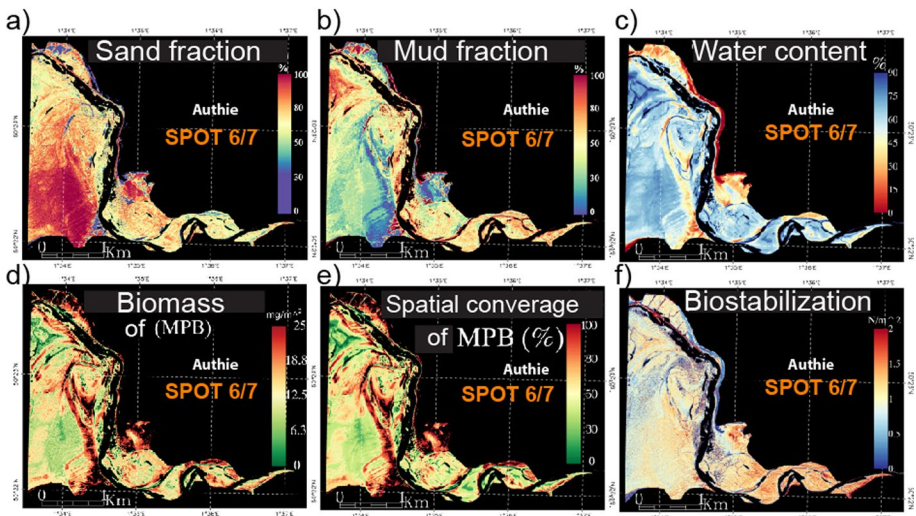

Fig. 7 Maps representing **a** sand and **b** mud, **c** water contents in %, **d** MPB biomass (mg.m^{-2}) spatial coverage of biofilm and biostabilization (N.m^{-2}) at low tide from SPOT 6/7 image in the Authie bay in the Northern France

6.2 Measurements of the Water Content: Suspended Sediment

The availability of High-Resolution Imagery with an increased revisit time (Landsat-8, Sentinel-2 and now Venμs) and relevant bio-optical algorithms (Han et al. 2016; Ngoc et al. 2020) opens the way to monitor suspended particulate matter (SPM) differences for rich turbid systems ranging from oligotrophic waters to ultra-turbid environments exceeding 1000 NTU. The advantage of high resolution in imagery is that the analyses can be done at the interface between continental and coastal zones where several small-scale phenomena can be observed at the land-sea interface (e.g., river discharges, plumes, turbidity front variation, flooding impact, gyres as a function of current, resuspended materials from intertidal domain, etc.). In monsoon-controlled regions such as in Vietnam, observed SPM patterns in Bach Dang estuary or Mekong Delta are changing drastically along the year and are clearly controlled by seasonal influence (Fig. 8).

Considering the sediment discharge to the ocean of the world's largest river-delta systems, Mouyen et al. (2018) demonstrated that it could be measured using data from the Gravity Recovery and Climate Experiment (GRACE) mission combined with a sediment transport model. This approach paves the way for a better quantitative monitoring of erosion in the delta basins. This new method should benefit from future generation of gravity measuring missions (GRACE Follow-On, NGGM/MAGIC project -NASA/ESA-, among others). Using Aqua Monitor database (Donchyts et al. 2016), a global-scale tool based on multiple Landsat missions (30-m resolution) showing where surface water changes occurred between 1985–2015, and hydrodynamic (wave, tide, river discharge) and sediment transport models, Nienhuis et al. (2020) investigated how much human activities have changed the dynamics of about 11,000 deltas worldwide. They concluded that, over the past 30 years, despite climate-related sea-level rise, deltas have globally experienced a net
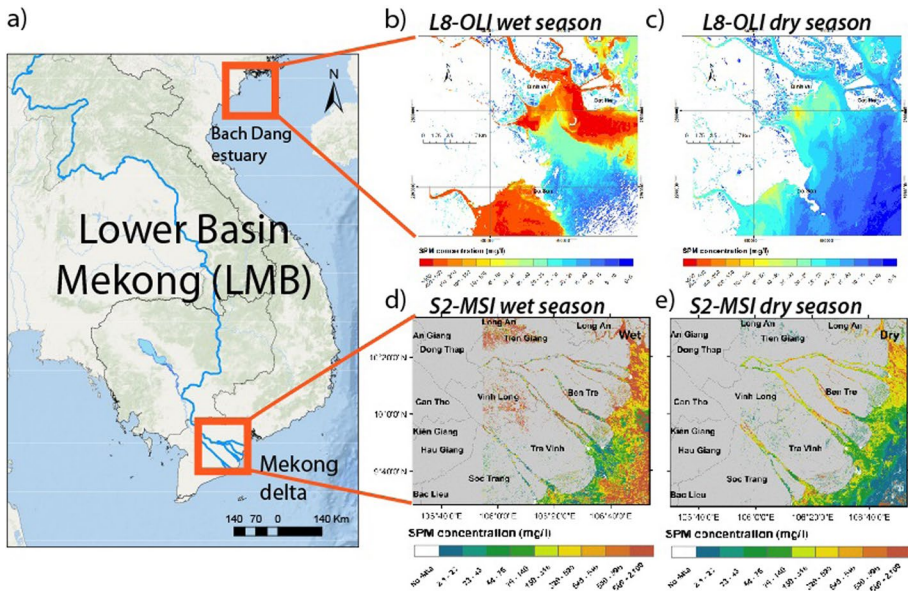

Fig. 8 Seasonal patterns comparison of SPM from L8-OLI images in **a** Bach Dang estuary during **b** dry and **c** wet seasons and from S2-MSI in Mekong delta during **d** dry and **e** wet seasons

land gain, with 25% of this gain being attributed to deforestation-induced increases in fluvial sediment supply.

In estuaries, one of the factors controlling the dynamics of fine sediment is the variation of the concentration in SPM both spatially and temporally (Jay et al. 2015; Hudson et al. 2017), resulting from complex transport, deposition, and erosion processes (Dyer 1988). These patterns are controlled by a large number of environmental factors including freshwater discharge, tide (especially in macrotidal environments), wind regime and flow turbulence (Jalón-Rojas et al. 2017; Uncles et al. 2006), as well as estuarine morphology (Grasso and Le Hir 2019). SPM spatio-temporal variability was widely analyzed in turbid coastal environments (e.g., estuaries and deltas) using medium resolution (250 m–1 km) multispectral images from MODIS and the Medium-Resolution Imaging Spectrometer (MERIS) sensors on-board satellite missions (e.g., Dogliotti et al. 2016; Doxaran et al. 2009; Hudson et al. 2017; Loisel et al. 2014). The launches of multi-spectral sensors operating at high spatial resolution—the Operational Land Imager (OLI) onboard Landsat-8 in 2013 (30 m) and MultisSpectral Instrument (MSI) onboard Sentinel-2A in 2015 and B in 2017 (10 m)— open a new era for SPM monitoring in terms of spatial resolution and image quality, allowing to study the SPM variability at unprecedented smaller scales from 10 to 100 m (Caballero et al. 2018; Normandin et al. 2019; Novoa et al. 2017). SPM is commonly retrieved from remotely-sensed surface reflectances from a wide range of approaches. Many of the mostly used are semi-analytical, based on the signatures of the SPM in the visible spectrum. One of the most popular is a semi-analytical algorithm linearly relating the ratio of the reflectance in the red and a linear combination of the inverse of this reflectance to the concentration in SPM. It allows to determine SPM concentration between 1 and 110 g/m^3 (Nechad et al. 2010). This approach was refined to extend its domain of validity. For instance, Han et al. (2016) proposed a multi-criteria approach calibrating the relationship from Nechad et al. (2010) for low to medium and high turbidity environments, allowing the retrieval of SPM concentrations from 0.15 to > 2,500 g/m^3. A threshold on the reflectance in the red is used to switch from a calibration to another. To limit the impact of the different calibrations a smoothing function is applied. This kind of approach can be calibrated globally (Han et al. 2016) or locally. In the latter case, a multi-criteria approach for low, medium and high turbidity environments was developed for the Gironde Estuary (Novoa et al. 2017). This approach was used to analyze the spatio-temporal patterns of SPM in the Gironde Estuary using Landsat-8 and Sentinel-2 images in response to environmental forcings and bathymetry (Normandin et al. 2019).

7 Monitoring Coastal Vegetation

The land-sea-continuum hosts a wide variety of coastal wetlands and submerged vegetation with types and structure that generally follows geomorphologic and environmental gradients such as bathymetry and salinity gradients. The local tidal amplitude, coastal topography and configuration of channel network dictate the extent of tidal propagation inland, with salinity gradients ranging from seawater to freshwater. These gradients give rise to an extraordinary, albeit vulnerable, diversity of plants such as seagrass meadows, salt and freshwater marshes (e.g., cattails, arrowheads, rushes), as well as mangrove and freshwater swamps (e.g., bald cypress, tupelo and ash). Seagrasses, mangroves and salt-marsh ecosystems are often referred to as blue carbon ecosystems due to their high carbon sequestration rates and contribution to the carbon cycle. Mangroves, salt marshes

and seagrasses globally cover approximately 138,000 km^2 (Bunting et al. 2018), 54,950 km^2 (Mcowen et al. 2017) and 160,390 km^2 (Mc Kenzie et al. 2020) respectively, providing services as well as livelihood to at least the half billion people living in those regions. Carbon sequestration is one of those services. Mangrove forests and salt marshes store 739 Mg C$_{org}$ ha^{-1} and 334 Mg C$_{org}$ ha^{-1} (Alongi 2020) with sequestration rates several times that of tropical and temperate forests per unit area. Although, they cover less than 1% of land surface, mangrove and salt marshes may contribute up to 34% of Dissolved Inorganic Carbon (DIC) export and 17% of Dissolved Organic carbon (DOC) and Particulate Organic carbon (POC) export to the world's coastal ocean (Alongi 2020).

Climate is another factor impacting the geographical distribution of plant type and allometry, with temperature and precipitation seasonality controlling plant productivity and phenological response. While most of these ecosystems are located at the mouth of coastal deltas and estuaries sheltered from sea actions, some blue carbon ecosystems are found seaward along protected coasts and islands.

Monitoring coastal vegetation from space offers significant challenges. These ecosystems are globally distributed (Fig. 9) but only cover a limited extent along coastline, and the diversity of plant structure and phenological requires specialized observation strategies and technologies. An ideal remote sensing instrument specific to the observation of coastal wetlands and submerged aquatic vegetation (SAV) traits should provide global coverage with high spatial resolution, and frequent revisit time that is commensurate to timescale of changes in the observable. These competing demands on the technology, compounded with the need for distinct observables presuppose a set of complementary remote sensing platforms to be used to monitor coastal wetlands and submerged aquatic vegetation.

Remote sensing has historically been used to characterize the spatial and temporal variability in the reflectance spectrum. These observations are particularly relevant to identify plant type distribution and estimate plant productivity, canopy cover fractions and above
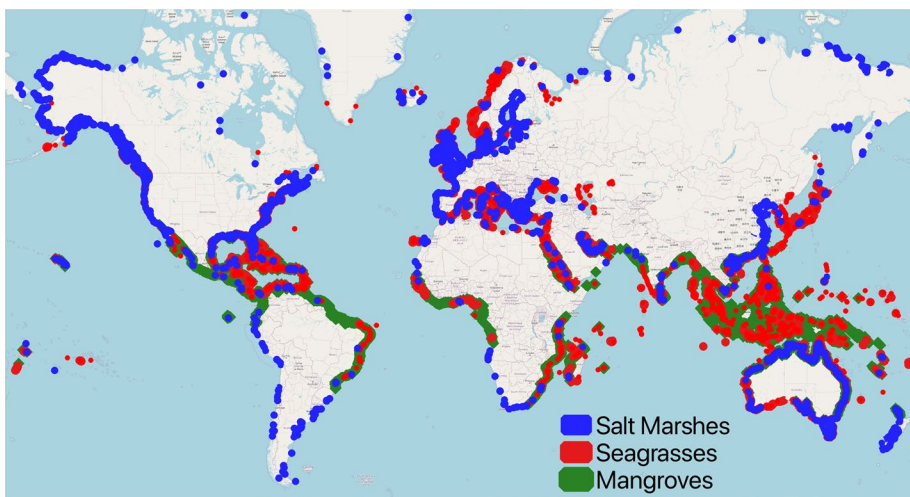

Fig. 9 Locations of the salt marshes (Mcowen et al. 2017), mangroves (Bunting et al. 2018) and seagrasses (UNEP-WCMC 2021) at the global scale

ground biomass. More recently, new remote sensing technologies were used to map vertical canopy structure (Simard et al. 2019) at global scale and even measure changes in water surface height in coastal wetlands (e.g., Wdowinski et al. 2008; Hong and Wdowinski 2013; Liao et al. 2020).

Passive multispectral sensors such as the Landsat series and MODIS measure reflectance within a set of spectral bands from which spectral indices can be derived (e.g., NDVI) to characterized spatial distribution and phenology across from local to global scales. These reflectance measurements also serve as input to models estimating geophysical observables such as vegetation specie distribution, Leaf Area Index (LAI), Above Ground Biomass (AGB) and the canopy cover fraction (CCF) (Guo et al. 2017). However, there has been limited success in accurately extracting geophysical characteristics in coastal wetlands with broad vegetation types being identified and limited AGB estimate (e.g., Byrd et al. 2018; Thomas et al. 2019). Better results are obtained focusing to local scales (e.g., Carle et al. 2014). Identification of SAV has proven to be even more challenging due to water turbidity (Rowan and Kalacska 2021), explaining the fact that global map of SAV have yet to be produced. Airborne imaging spectrometers were shown to outperform multispectral instrument when classifying land cover in these complex coastal landscape (Carle et al. 2014).

To date, the greatest challenges appear to be mapping the extent of SAV, delimiting the smooth transition between salt and fresh water vegetation, and monitoring coastal regions with persistent cloud cover. While radar remote sensing solves the cloud cover issue that is particularly prevalent in coastal regions, it is limited to identify and detect changes in general vegetation structure and landscape patterns. Radar has been used to map mangrove forest extent and change (Bunting et al. 2018). It is also helpful in mapping coastal wetlands (e.g., Byrd et al. 2018). However, as electromagnetic waves do not penetrate water and thus cannot be used to map submerged vegetation. Synthetic Aperture Radar Interferometry (InSAR) provides the most exciting measurements.

Plant vertical structure is an important parameter to estimate AGB, productivity and carbon stocks, as well as to characterize habitat function. InSAR, LiDAR and stereophotogrammetry are three technologies that enable measurement of height. InSAR with a non-zero baseline (i.e., a pair of radar images are obtained from slightly different point of view) is typically used to map surface topography (Rizzoli et al. 2017; Farr et al. 2007) relative to the Earth ellipsoid, effectively producing Digital Surface Models (DSMs). Since radar has limited penetration into forest canopies, the observed DSM represented the so-called inSAR phase center, which is located within the canopy. And because coastal wetlands reside around mean sea level, inSAR DSMs have been used to map mangrove canopy height (Simard et al. 2019). A more recent technique called Polarimetric InSAR (or polinSAR) estimates forest canopy height in addition to emerged ground topography. The InSAR observations at different polarizations result from different microwave scattering mechanisms and are used within a simple model to invert height (height), without the need for knowledge of ground topography. LiDAR is the most well-known remote sensing technology to measure forest structure. It has been used to map canopy structure, water surface elevation and bathymetry of coastal wetlands. LiDAR typically operate in the near infrared NIR (1064 nm) or green wavelength (~ 532 nm) to generate pseudo images by gathering a collection of point measurements within a swath. LiDAR systems provide the most accurate measurements of surface elevation and can be used to map vertical structure of marsh vegetation and mangrove forests. The potential for green light to penetrate low turbidity water can provide bathymetry (e.g., Gong et al. 2021) to approximately 10 m in very clear water cases (e.g., Thomas et al. 2021). These same green LiDAR measurements can be used to map the structure of SAV that are known to be present.

8 Conclusions and Future Prospects

8.1 Conclusions

Coastal environments (including estuaries and deltas) are areas with very important ecological end economic issues, strongly affected by anthropogenic impact and climate change. Thus, they are affected by multiple hazards (storm surges, heavy rains, coastal river floods, inundations, coastline erosion/retreat, pollutions…) which will intensify in the context of climate change. The sustainable future for coastal zones depends on our capacity to better understand, manage and predict the evolution of these environments. This requires us to monitor the hydrodynamics and the evolution of the morphology, sedimentology and biology of these diverse environments which are impacted by a variety of natural and anthropic environmental changes.

However, controlling the coastal and estuarine dynamics is largely complex since they are subject to high spatial and temporal variability different hydrodynamic, morphological, sedimentological and biological processes, that act at various spatial and temporal scales.

Under the complexities of these zones, the measurements of these processes are limited and not enough to fully understand their spatial and time variability, which is only addressed by numerical models calibrated and validated with a few widely spaced in-situ measurements and local field campaigns.

In recent years, the observation of coastal environments by satellites has made significant progress in connection with the improvement of their resolution, a more frequent revisit, the combined use of several sensors and the use of altimetry data closer to the coastline. In fact, the interest of satellite data focuses on providing spatialized 2D information and can use different techniques (Optical imagery, Altimetry, Microwave radar, Interferometric Synthetic Aperture Radar, Infrared, Near Infrared, etc.) in order to allow the measurement of different physical quantities with the aim of providing highly resolved coverage of the driving physical processes at different space and time scales. These advances play a key role in improving our understanding of the estuarine, deltaic and coastal environments.

For example, over the last two decades, satellite radar altimeters, measuring sea level variations, have provided major advances in ocean science, and the monitoring of the coastal zone with satellite altimetry is nowadays a requirement of the most recent missions. The critical need to use radar altimetry in the coastal zone have fostered tremendous improvements in the recent years and allows today to measure with precision up to less than 5 km near the coastline several processes such as the sea level, current, wind-waves and waves and storm surges.

In optical imagery, as time has progressed, the pixel size of publicly available images has decreased from 80 m for the first Landsat missions 1–3 (1972–1983), to 30 m for Landsat 4–8 (1982—present), 10 m for Sentinel-2 (2015—present) and 0.5 m for Pleiades. At the same time, the satellite revisit period has decreased from every 18 days for Landsat 1–3, to 16 days for Landsat 4–8 and 5 days for Sentinel-2. In addition, we can cite IKONOS, Quickbird, or other private initiatives based on nano-satellites (e.g., SkySat, with a metric resolution and daily revisit period).

These improvements both of the resolution and revisit have allowed significant progress in monitoring of the shoreline and now offer a good alternative for DEM construction for the beaches and the intertidal areas and bathymetry for depths up to 40–60 m over large spatial areas with sufficient resolution and unprecedented accuracy. Bathymetric inversion codes developed from wave dispersion relationships make use of the

temporal information contained in the spatial images and were applied to different satellite observations (IKONOS, WorldView-2, SPOT5/6, Sentinel-2 and Pleiades) with unprecedented accuracy when applied at regional scale. For the beaches and intertidal areas, it is crucial to keep the acquisition period as short as possible and to determine the optimal combination between the acquisition period and a complete sampling of the tidal cycle to construct DEM. Nowadays, owing to the deployment of Sentinel-1 and Sentinel-2 missions, short acquisition periods (~ 3 months) are more easily achievable.

Moreover, bathymetry and topography from data satellite can be combined in the same vertical reference to generate a continuum land sea DSM (Digital Surface Models). This is clearly the way forward for coastal studies to model the hydrodynamic and flooding with numerical simulations and to document exchanges of sediment between the lower and upper shoreface and monitor topographic changes and estimate sediment budgets. On the other hand, although Vertical Land Motion (VLM) measurements remain a challenging issue, the advances in satellite-based techniques, such as InSAR, GNSS (Global Navigation Satellite System) and satellite altimetry combining with tide gauges allow the measurement of VLMs at local to regional scales.

Otherwise, the use of optical imaging including multispectral and hyperspectral systems is well suited for improving our understanding of the sediment dynamics in response to physical forcing or biological mechanisms and also provides a synoptic overview of bio-physical characteristics of sediments over estuarine and deltas systems.

The availability of High-Resolution imagery with an increased revisit time (Landsat-8, Sentinel-2 and now Venµs) and relevant bio-optical algorithms opens the way to monitor suspended particulate matter (SPM) differences for rich turbid systems ranging from oligotrophic waters to ultra-turbid environments.

Moreover, multispectral sensors have been also used to identify the land cover types and classify the distribution of the vegetation density and the sediment characteristics from the spectral response of the systems. The passive multispectral sensors such as the Landsat series and MODIS measure reflectance within a set of spectral bands from which spectral indices can be derived (e.g., NDVI) to characterized spatial distribution of submerged aquatic vegetation and phenology across from local to global scales.

All the satellite data from the combination of several sensors and modeling can lead to the calculation of vulnerability and risk indices for populations and infrastructures in response to climatic hazards and the mapping of these indices in the coastal araes. For example, the vulnerable and risk zones on the basis of the shoreline change and the coastal vulnerability index (CVI) which includes six vulnerable parameters, namely coastal morphology, shoreline change rate, coastal slope, relative sea level change, mean wave height and mean tide range. The coastal morphology (DEM), shoreline change rate, coastal slope can be obtained from optical imagery and relative sea level change from altimetry, mean wave height and mean tide range from modeling.

8.2 Perspectives

The hydrodynamics in the coastal, estuarine and delta regions is very complex because this is subject to high spatial and temporal variability in water levels, linked to interactions between different phenomena such as offshore and coastal currents, upwelling/downwelling, waves (with runup and overtopping), tides, storm surges, discharge from streamflow and groundwater, sea level rise in the context of climate change and vertical land motion that act at various spatial and temporal scales.

The key role of the different hydrodynamic forcing in the physical interactions within the coastal, estuarine and deltaic areas remains poorly known and not fully resolved by numerical modeling. Under the complexities of these zones, the hydrodynamic measurements are limited and not enough to fully understand the spatial variability of water levels, which is only addressed by numerical models calibrated and validated with a few widely spaced in-situ measurements.

The challenge of altimetry in coastal areas is the provision of time series of water levels as close as possible to the coast, in the same way as those provided for the oceans or in hydrology on the world's major rivers or lakes. The recent rapid increase in the number of altimetry satellites in orbit simultaneously and the evolution of the altimetry measurement from a one-dimensional profile to a two dimensional swath are promising advances that aid the production of seamless sea level estimations and change the perspective of the coastal altimetry from a sensor that was systematically flagged 50 km away from the coast to a safe scientific exploitation of the data up to at least 3 km from the coastline. The possibility to use individual echoes from CryoSat-2 and Sentinel-3 has demonstrated the potential of novel processing methods at land-sea interface by applying coherent integration of some/many echoes (e.g., Egido and Smith 2016; Abileah and Vignudelli 2021). Regardless of how new and advanced technology and data processing are, it is obvious that when getting closer to the coast a more careful quality control of the data is needed. Only further progress using high resolution tidal models can help overcome this issue. Another piece of information that is key in estimating sea level anomalies is the mean sea surface that is usually computed using datasets that are not suitable for the coastal zone. It must also be noted that, when going near coasts, users rely on along track data. Given the local characteristics of the phenomena to be observed, having data along tracks only is a problem, since it is unknown what happens between the repeating tracks. There is a need of merging altimeter observations from the various missions, as it happens in open ocean., therefore, new ideas for that in the coastal zone are necessary.

Otherwise, in the coastal regions and, specifically along tropical delta coasts, which are still non-instrumented or insufficiently instrumented with tide-gauges and collocated GNSS stations, there remains today a knowledge gap in understanding coastal sea level changes. Moreover, for these deltas, the VLM is a key part of their future survival and several studies showed that most major river deltas are now sinking. For these areas which are still non-instrumented or insufficiently instrumented, the space missions will continue to supply unprecedentedly precise observations of sea level changes (e.g., the satellite missions Sentinel-6/Jason-CS, Sentinel-3C/D, SWOT). The highest priority should be given to the development of fully integrated multidisciplinary observing systems, including a greater number of tide gauges and co-located GNSS networks, and precise satellite altimetry data for these low-lying highly populated coastlines. In fact, understanding of the sea level critical thresholds along low-lying highly populated coastlines are vital societal issues. This issue needs to be addressed in order to provide accurate information to decision-makers and to allow elaboration of efficient adaptive strategies.

On the other hand, the interactions between water reservoirs (sea, river, groundwater) and the associated processes and the interactions between the hydrodynamic, morphology, sedimentology and biology should be better understood by the combined use of several sensors (Optical imagery, Altimetry, Microwave radar, Interferometric Synthetic Aperture Radar, Infrared, Near Infrared, etc.) and the space and time resolution of the satellite is a key issue. The combined use of these different techniques in order to

allow the measurement of different physical quantities with the aim of providing highly-resolved coverage of the driving physical processes at different space and time scales is still insufficient and will have to be further developed to better manage and predict the evolution of the coastal environment and to protect the population who live near the shoreline. For example, the space resolution and the revisit of the satellite is a key issue to monitor the small scale hydrodynamic processes not yet resolved by satellites, such as the combining of extreme events (storm surges, river floods) with tidal information.

Otherwise, the construction of accurate DEM of the topography of the beaches and intertidal zones and shallow water bathymetry in the continuum land sea is still exploratory and needs more investigation. This is essential for hydrodynamic modeling, quantification of fine coastal processes such as the run up in swash zone and infragravity waves, to quantify the exchanges of sediment between the lower and upper shoreface and monitor topographic changes and estimate sediment budgets.

In fact, only a small fraction of world's coasts is surveyed by hydrographic and geographic national services, and nautical charts and DEMs are decades old. This leads to severe uncertainty in the risk assessment and forecast of storms, coastal river floods, and climate changes impact. Characterization of physical properties of the coastal zone is thus needed for coastal hazard assessments.

The definition of vulnerability and risk indices for populations and infrastructures in response to climatic hazards requires the combined use of several satellite sensors, other remote sensing sensors (such as Lidar, Video and IR camera, video and IR by drone), in-situ measurements (tides gauges, GNSS…) and modeling.

The processing and the combination of all these data will require the development of new high-resolution algorithms and the use of new approaches such as Deep Learning. In fact, the Deep Learning techniques open new strong perspectives to map the change of the shoreline and coastal features from the satellite.

All data of the different satellite sensors should be integrated in an observatory of the coastal zones (including estuaries and deltas) to provide useful and needed information for authorities and stakeholders for coastal management and implementation of ecosystem protection policies.

Author Contributions BL and SV designed and drafted the manuscript. MB, AB, JB, FB, FF, DI, ES, MP, MM, MS, IT and CV contributed to the different sections of the manuscript.

Declarations

Conflict of interest The authors have no competing interests to declare that are relevant to the content of this article.

permitted by statutory regulation or exceeds the permitted use, you will need to obtain permission directly from the copyright holder. To view a copy of this licence, visit http://creativecommons.org/licenses/by/4.0/.

References

Aarninkhof SGJ, Turner IL, Dronkers TDT, Caljouw M, Nipius L (2003) A video-based technique for mapping intertidal beach bathymetry. Coast Eng 49(4):275–289. https://doi.org/10.1016/S0378-3839(03)00064-4

Abdalla S (2012) Ku-band radar altimeter surface wind speed algorithm. Mar Geod 35(sup1):276–298. https://doi.org/10.1080/01490419.2012.718676

Abidin HZ, Andreas H, Gumilar I, Brinkman JJ (2015) Study on the risk and impacts of land subsidence in Jakarta. Proc Int Assoc Hydrol Sci 372:115–120. https://doi.org/10.5194/piahs-372-115-2015

Abileah R, Vignudelli S (2021) Precise inland surface altimetry (PISA) with nadir specular echoes from Sentinel-3: algorithm and performance assessment. Remote Sens Environ 264:112580. https://doi.org/10.1016/j.rse.2021.112580

Abileah R (2006) Mapping shallow water depth from satellite. In: Proceedings of the ASPRS annual conference, Reno, Nevada, pp 1–7. http://www.asprs.org/a/publications/proceedings/reno2006/0001.pdf

Adam S, De Backer A, De Wever A, Sabbe K, Toorman EA, Vincx M, Monbaliu J (2011) Bio-physical characterization of sediment stability in mudflats using remote sensing: a laboratory experiment. Cont Shelf Res 31(10):S26–S35. https://doi.org/10.1016/j.csr.2009.12.008

Agardy T, Alder J (2005) Coastal systems. Ecosystems and human well-being: current state and trends. Island Press, Washington, DC, pp 513–550

Al Najar M, Thoumyre G, Bergsma EW, Almar R, Benshila R, Wilson DG (2021) Satellite derived bathymetry using deep learning. Mach Learn. https://doi.org/10.1007/s10994-021-05977-w

Allison M, Yuill B, Törnqvist T, Amelung F, Dixon T, Erkens G, Stuurman R, Jones C, Milne G, Steckler M, Syvitski J (2016) Global risks and research priorities for coastal subsidence. Eos, vol 97. Washington, DC. https://doi.org/10.1029/2016EO055013

Almar R, Bergsma EWJ, Maisongrande P, de Almeida LPM (2019) Wave-derived coastal bathymetry from satellite video imagery: a showcase with Pleiades persistent mode. Remote Sens Environ 231:111263. https://doi.org/10.1016/J.RSE.2019.111263

Almeida LP, Almar R, Bergsma EW, Berthier E, Baptista P, Garel E, Dada OA, Alves B (2019) Deriving high spatial-resolution coastal topography from sub-meter satellite stereo imagery. Remote Sens 11(5):590. https://doi.org/10.3390/rs11050590

Alongi DM (2020) Carbon cycling in the world's mangrove ecosystems revisited: significance of non-steady state diagenesis and subsurface linkages between the 4 forest floor and the coastal ocean. Forests 11:977

Anthony EJ, Aagaard T (2020) The lower shoreface: morphodynamics and sediment connectivity with the upper shoreface and beach. Earth Sci Rev 210:103334. https://doi.org/10.1016/j.earscirev.2020.103334

Arbic BK, Lyard F, Ponte A, Ray RD, Richman JG, Shriver JF, Zaron E, Zhao Z (2014) Tides and the SWOT mission: transition from science definition team to science team. Civil and Environmental Engineering Faculty Publications and Presentations. 336. http://archives.pdx.edu/ds/psu/16710

Arns A, Wahl T, Dangendorf S, Jensen J, Pattiaratchi C (2017) Sea-level rise induced amplification of coastal protection design heights. Sci Rep 7(1):1–9. https://doi.org/10.1038/srep40171

Astudillo O, Dewitte B, Mallet M, Frappart F, Rutllant JA, Ramos M, Bravo L, Goubanova K, Illig S (2017) Surface winds off Peru-Chile: observing closer to the coast from radar altimetry. Remote Sens Environ 191:179–196. https://doi.org/10.1016/j.rse.2017.01.010

Astudillo O, Dewitte B, Mallet M, Rutllant JA, Goubanova K, Frappart F, Ramos M, Bravo L (2019) Sensitivity of the near-shore oceanic circulation off Central Chile to coastal wind profiles characteristics. J Geophys Res Ocean 124(7):4644–4676. https://doi.org/10.1029/2018JC014051

Ballu V, Gravelle M, Wöppelmann G, de Viron O, Rebischung P, Becker M, Sakic P (2019) Vertical land motion in the Southwest and Central Pacific from available GNSS solutions and implications for relative sea levels. Geophys J Int 218(3):1537–1551. https://doi.org/10.1093/gji/ggz247

Bamler R, Hartl P (1998) Synthetic aperture radar interferometry. Inverse Probl 14(4):R1

Basco D (1991) Boundary conditions and long-term shoreline change rates for the southern Virginia ocean coastline. Shore Beach 59(4):8–13. https://doi.org/10.1061/9780872627765.099

Becker M, Papa F, Karpytchev M, Delebecque C, Krien Y, Khan JU, Ballu V, Durand F, Le Cozannet G, Islam AS, Calmant S (2020) Water level changes, subsidence, and sea level rise in the

Ganges–Brahmaputra–Meghna delta. Proc Natl Acad Sci 117(4):1867–1876. https://doi.org/10.1073/pnas.1912921117

Becker M, Karpytchev M, Papa F (2019) Hotspots of relative sea level rise in the tropics. In: Venugopal V, Sukhatme J, Murtugudde R, Roca R (eds) Tropical extremes, pp 203–262. https://doi.org/10.1016/B978-0-12-809248-4.00007-8

Benveniste J, Cazenave A, Vignudelli S, Fenoglio-Marc L, Shah R, Almar R, Andersen O, Birol F, Bonnefond P, Bouffard J, Calafat F, Cardellach E, Cipollini P, Le Cozannet G, Dufau C, Fernandes MJ, Frappart F, Garrison J, Gommenginger C, Han G, Høyer JL, Kourafalou V, Leuliette E, Li Z, Loisel H, Madsen KS, Marcos M, Melet A, Meyssignac B, Pascual A, Passaro M, Ribó S, Scharroo R, Song YT, Speich S, Wilkin J, Woodworth P, Wöppelmann G (2019) Requirements for a coastal hazards observing system. Front Mar Sci 6:348. https://doi.org/10.3389/fmars.2019.00348

Benveniste J, Birol F, Calafat F, Cazenave A, Dieng H, Gouzenes Y, Legeais JF, Léger F, Niño F, Passaro M, Schwatke C, Shaw A, (The Climate Change Initiative Coastal Sea Level Team) (2020a) Coastal sea level anomalies and associated trends from Jason satellite altimetry over 2002–2018. Nat Sci Data 7:357. https://doi.org/10.1038/s41597-020-00694-w

Benveniste J, Mandea M, Melet A, Ferrier P (2020b) Earth observations for coastal hazards monitoring and international services: a European perspective. Surv Geophys 41(6):1185–1208. https://doi.org/10.1007/s10712-020-09612-6

Bergsma E, Almar R, Maisongrande P (2019) Radon-augmented sentinel-2 satellite imagery to derive wave-patterns and regional bathymetry. Remote Sens 11(16):1918

Bergsma EW, Almar R (2020) Coastal coverage of ESA'Sentinel 2 mission. Adv Space Res 65(11):2636–2644. https://doi.org/10.1016/j.asr.2020.03.001

Bergsma EW, Almar R, Rolland A, Binet R, Brodie KL, Bak AS (2021) Coastal morphology from space: a showcase of monitoring the topography-bathymetry continuum. Remote Sens Environ 261:112469. https://doi.org/10.1016/j.rse.2021.112469

Besset M, Anthony EJ, Bouchette F (2019) Multi-decadal variations in delta shorelines and their relationship to river sediment supply: an assessment and review. Earth Sci Rev 193:199–219. https://doi.org/10.1016/j.earscirev.2019.04.018

Biancamaria S, Lettenmaier DP, Pavelsky TM (2016) The SWOT mission and its capabilities for land hydrology. Surv Geophys 37:307–337. https://doi.org/10.1007/s10712-015-9346-y

Birol F, Cancet M, Estournel C (2010) Aspects of the seasonal variability of the Northern Current (NW Mediterranean Sea) observed by altimetry. J Mar Syst 81(4):297–311. https://doi.org/10.1016/j.jmarsys.2010.01.005

Birol F, Niño F (2015) Ku and Ka-band altimeter data in the northwestern mediterranean sea. Mar Geod 38:313–327. https://doi.org/10.1080/01490419.2015.1034814

Birol F, Léger F, Passaro M, Cazenave A, Niño F, Calafat FM, Shaw A, Legeais JF, Gouzenes Y, Schwatke C, Benveniste J (2021) The X-TRACK/ALES multi-mission processing system: new advances in altimetry towards the coast. Adv Space Res 67(8):2398–2415. https://doi.org/10.1016/j.asr.2021.01.049

Bishop-Taylor R, Sagar S, Lymburner L, Alam I, Sixsmith J (2019) Sub-pixel waterline extraction: characterising accuracy and sensitivity to indices and spectra. Remote Sens 11(24):2984. https://doi.org/10.3390/rs11242984

Boak EH, Turner IL (2005) Shoreline definition and detection: a review. J Coast Res 21(4):688–703. https://doi.org/10.2112/03-0071.1

Bouffard J, Vignudelli S, Cipollini P, Menard Y (2008) Exploiting the potential of an improved multimission altimetric data set over the coastal ocean. Geophys Res Lett. https://doi.org/10.1029/2008GL033488

Brown G (1977) The average impulse response of a rough surface and its applications. IEEE Trans Antennas Propag 25(1):67–74. https://doi.org/10.1109/TAP.1977.1141536

Buddemeier RW, Smith SV, Swaney DP, Crossland CJ (2002) The role of the coastal ocean in the disturbed and undisturbed nutrient and carbon cycles. LOICZ Rep Stud 24:84

Bunting P, Rosenqvist A, Lucas RM, Rebelo LM, Hilarides L, Thomas N, Hardy A, Itoh T, Shimada M, Finlayson CM (2018) The global mangrove watch—a new 2010 global baseline of mangrove extent. Remote Sens 10(10):1669. https://doi.org/10.3390/rs10101669

Byrd KB, Ballanti L, Thomas N, Nguyen D, Holmquist JR, Simard M, Windham-Myers L (2018) A remote sensing-based model of tidal marsh aboveground carbon stocks for the conterminous United States. ISPRS J Photogramm Remote Sens 139:255–271

Caballero I, Stumpf RP (2019) Retrieval of nearshore bathymetry from Sentinel-2A and 2B satellites in South Florida coastal waters. Estuar Coast Shelf Sci 226:106277. https://doi.org/10.1016/j.ecss.2019.106277

Caballero I, Steinmetz F, Navarro G (2018) Evaluation of the first year of operational Sentinel-2A data for retrieval of suspended solids in medium-to high-turbidity waters. Remote Sens 10(7):982

Cancet M, Andersen O, Abulaitijiang A, Cotton D, Benveniste J (2019) Improvement of the arctic ocean bathymetry and regional tide atlas: first result on evaluating existing arctic ocean bathymetric models. Fiducial reference measurements for altimetry. Springer, Cham, pp 55–63. https://doi.org/10.1007/1345_2019_85

Carle MV, Wang L, Sasser CE (2014) Mapping freshwater marsh species distributions using WorldView-2 high-resolution multispectral satellite imagery. Int J Remote Sens 35(13):4698–4716. https://doi.org/10.1080/01431161.2014.919685

Carrère L, Lyard F (2003) Modeling the barotropic response of the global ocean to atmospheric wind and pressure forcing-comparisons with observations. Geophys Res Lett. https://doi.org/10.1029/2002GL016473

Carret A, Birol F, Estournel C, Zakardjian B, Testor P (2019) Synergy between in situ and altimetry data to observe and study Northern Current variations (NW Mediterranean Sea). Ocean Sci 15(2):269–290. https://doi.org/10.5194/os-15-269-2019

Castelle B, Masselink G, Scott T, Stokes C, Konstantinou A, Marieu V, Bujan S (2021) Satellite-derived shoreline detection at a high-energy meso-macrotidal beach. Geomorphology 383:107707. https://doi.org/10.1016/j.geomorph.2021.107707

Charles E, Idier D, Thiébot J, Le Cozannet G, Pedreros R, Ardhuin F, Planton S (2012) Present wave climate in the Bay of Biscay: spatiotemporal variability and trends from 1958 to 2001. J Clim 25:2020–2039. https://doi.org/10.1175/JCLI-D-11-00086.1

Chaussard E, Amelung F, Abidin H, Hong SH (2013) Sinking cities in Indonesia: ALOS PALSAR detects rapid subsidence due to groundwater and gas extraction. Remote Sens Environ 128:150–161. https://doi.org/10.1016/j.rse.2012.10.015

Choi C, Kim DJ (2018) Optimum baseline of a single-pass In-SAR system to generate the best DEM in tidal flats. IEEE J Sel Top Appl Earth Obs Remote Sens 11(3):919–929. https://doi.org/10.1109/JSTARS.2018.2795107

Choung YJ, Jo MH (2017) Comparison between a machine-learning-based method and a water-index-based method for shoreline mapping using a high-resolution satellite image acquired in Hwado Island, South Korea. J Sens. https://doi.org/10.1155/2017/8245204

Cohn N, Ruggiero P (2016) The influence of seasonal to interannual nearshore profile variability on extreme water levels: modeling wave runup on dissipative beaches. Coast Eng 115:79–92. https://doi.org/10.1016/j.coastaleng.2016.01.006,10.1016/j.coastaleng.2016.01.006

Collin A, Hench JL, Pastol Y, Planes S, Thiault T, Schmitt RJ, Holbrook SJ, Davies N, Troyer M (2018) High resolution topobathymetry using a Pleiades-1 triplet: Moorea Island in 3D. Remote Sens Environ 208:109–119. https://doi.org/10.1016/j.rse.2018.02.015

Combe JP, Launeau P, Carrère V, Despan D, Méléder V, Barillé L, Sotin C (2005) Mapping microphytobenthos biomass by non-linear inversion of visible-infrared hyperspectral images. Remote Sens Environ 98(4):371–387. https://doi.org/10.1016/j.rse.2005.07.010

Daly C, Baba W, Bergsma E, Thoumyre G, Almar R, Garlan T (2022) The new era of regional coastal bathymetry from space: A showcase for West Africa using optical Sentinel-2 imagery. Remote Sens Environ 278:113084

Danilo C, Binet R (2013) Bathymetry estimation from wave motion with optical imagery: influence of acquisition parameters. In: 2013 MTS/IEEE OCEANS-Bergen, IEEE, pp 1–5. https://doi.org/10.1109/OCEANS-Bergen.2013.6608068

Danilo C, Melgani F (2019) High-coverage satellite-based coastal bathymetry through a fusion of physical and learning methods. Remote Sens 11(4):376. https://doi.org/10.3390/rs11040376

De Schipper MA, de Vries S, Ruessink G, de Zeeuw RC, Rutten J, van Gelder-Maas C, Stive MJ (2016) Initial spreading of a mega feeder nourishment: observations of the sand engine pilot project. Coast Eng 111:23–38. https://doi.org/10.1016/j.coastaleng.2015.10.011

de Vries H, Breton M, de Mulder T, Krestenitis Y, Ozer J, Proctor R, Ruddick K, Salomon J, Voorrips A (1995) A comparison of 2Dstorm surge models applied to three shallow European seas. Environ Softw 10(1):23–42

Dewidar KH, Frihy O (2007) Pre-and post-beach response to engineering hard structures using Landsat time-series at the northwestern part of the Nile delta. Egypt J Coast Conserv 11(2):133–142. https://doi.org/10.1007/s11852-008-0013-z

Dodet G, Mélet A, Ardhuin F, Bertin X, Idier D, Almar R (2019) The contribution of wind-generated waves to coastal sea-level changes. Surv Geophys 40(6):1563–1601. https://doi.org/10.1007/s10712-019-09557-5

Dogliotti AI, Ruddick K, Guerrero R (2016) Seasonal and inter-annual turbidity variability in the Río de la Plata from 15 years of MODIS: El Niño dilution effect. Estuar Coast Shelf Sci 182:27–39. https://doi.org/10.1016/j.ecss.2016.09.013

Donchyts G, Baart F, Winsemius H, Gorelick N, Kwadijk J, Van De Giesen N (2016) Earth's surface water change over the past 30 years. Nat Clim Chang 6(9):810–813. https://doi.org/10.1038/nclimate3111

Doxaran D, Froidefond JM, Castaing P, Babin M (2009) Dynamics of the turbidity maximum zone in a macrotidal estuary (the Gironde, France): observations from field and MODIS satellite data. Estuar Coast Shelf Sci 81(3):321–332. https://doi.org/10.1016/j.ecss.2008.11.013

Dyer KR (1988) Fine sediment particle transport in estuaries. Physical processes in estuaries. Springer, Berlin, Heidelberg, pp 295–310. https://doi.org/10.1007/978-3-642-73691-9_16

Egido A, Smith WH (2016) Fully focused SAR altimetry: theory and applications. IEEE Trans Geosci Remote Sens 55(1):392–406. https://doi.org/10.1109/TGRS.2016.2607122

El Banna MM, Hereher ME (2009) Detecting temporal shoreline changes and erosion/accretion rates, using remote sensing, and their associated sediment characteristics along the coast of North Sinai. Egypt Environ Geol 58(7):1419–1427. https://doi.org/10.1007/s00254-008-1644-y

Elnabwy MT, Elbeltagi E, El Banna MM, Elshikh MM, Motawa I, Kaloop MR (2020) An approach based on landsat images for shoreline monitoring to support integrated coastal management—a case study, Ezbet Elborg, Nile Delta. Egypt ISPRS Int J Geo-Inf 9(4):199. https://doi.org/10.3390/ijgi9040199

Elsayed SM, Oumeraci H (2017) Effect of beach slope and grain-stabilization on coastal sediment transport: an attempt to overcome the erosion overestimation by XBeach. Coast Eng 121:179–196. https://doi.org/10.1016/j.coastaleng.2016.12.009

Erban LE, Gorelick SM, Zebker HA (2014) Groundwater extraction, land subsidence, and sea-level rise in the Mekong Delta. Vietnam Environ Res Lett 9(8):084010. https://doi.org/10.1088/1748-9326/9/8/084010

Ericson JP, Vörösmarty CJ, Dingman SL, Ward LG, Meybeck M (2006) Effective sea-level rise and deltas: causes of change and human dimension implications. Glob Planet Chang 50(1–2):63–82. https://doi.org/10.1016/j.gloplacha.2005.07.004

Ettritch G, Hardy A, Bojang L, Cross D, Bunting P, Brewer P (2018) Enhancing digital elevation models for hydraulic modelling using flood frequency detection. Remote Sens Environ 217:506–522. https://doi.org/10.1016/j.rse.2018.08.029

Evagorou E, Mettas C, Agapiou A, Themistocleous K, Hadjimitsis D (2019) Bathymetric maps from multi-temporal analysis of Sentinel-2 data: the case study of Limassol, Cyprus. Adv Geosci 45:397–407. https://doi.org/10.5194/adgeo-45-397-2019

Familkhalili R, Talke SA (2016) The effect of channel deepening on tides and storm surge: a case study of Wilmington. NC Geophys Res Lett 43(17):9138–9147. https://doi.org/10.1002/2016GL069494

Fang J, Sun S, Shi P, Wang JA (2014) Assessment and mapping of potential storm surge impacts on global population and economy. Int J Disaster Risk Sci 5(4):323–331. https://doi.org/10.1007/s13753-014-0035-0

Farr TG, Rosen PA, Caro E, Crippen R, Duren R, Hensley S, Kobrick M, Paller M, Rodriguez E, Roth L, Seal D (2007) The shuttle radar topography mission. Rev Geophys. https://doi.org/10.1029/2005RG000183

Fenoglio-Marc L (2002) Long-term sea level change in the Mediterranean Sea from multi-satellite altimetry and tide gauges. Phys Chem Earth Parts A/B/C 27(32–34):1419–1431. https://doi.org/10.1016/S1474-7065(02)00084-0

Fenoglio-Marc L, Schöne T, Illigner J, Becker M, Manurung P, Khafid (2012) Sea level change and vertical motion from satellite altimetry, tide gauges and GPS in the Indonesian region. Mar Geod 35(sup1):137–150. https://doi.org/10.1080/01490419.2012.718682

Fenster MS, Dolan R, Elder JF (1993) A new method for predicting shoreline positions from historical data. J Coast Res 9(1):147–171

Fernandes MJ, Lázaro C, Nunes AL, Scharroo R (2014) Atmospheric corrections for altimetry studies over inland water. Remote Sens 6(6):4952–4997. https://doi.org/10.3390/rs6064952

Fernandes MJ, Lázaro C, Vieira T (2021) On the role of the troposphere in satellite altimetry. Remote Sens Environ 252:112149. https://doi.org/10.1016/j.rse.2020.112149

Fu LL, Chelton DB (2001) Large-scale ocean circulation. In: Fu L-L, Cazenave A (eds) Satellite altimetry and earth sci-ences: a handbook for techniques and applications, vol 423. Academic Press, San Diego, pp 133–16

Fu LL, Alsdorf D, Morrow R, Rodriguez E, Mognard N (2012) SWOT: the surface water and ocean topography mission: wide-swath altimetric elevation on Earth. Jet Propulsion Laboratory, National Aeronautics and Space Administration, Pasadena, CA. http://hdl.handle.net/2014/41996

Fu LL, Ubelmann C (2014) On the transition from profile altimeter to swath altimeter for observing global ocean surface topography. J Atmos Ocean Technol 31(2):560–568. https://doi.org/10.1175/JTECH-D-13-00109.1

Gainza J, Rueda A, Camus P, Tomás A, Méndez FJ, Sano M, Tomlinson R (2018) A meta-modelling approach for estimating long-term wave run-up and total water level on beaches. J Coast Res 34:475–489

Gao J (2009) Bathymetric mapping by means of remote sensing: methods, accuracy and limitations. Prog Phys Geogr 33(1):103–116. https://doi.org/10.1177/0309133309105657

Gao S (2019) Geomorphology and sedimentology of tidal flats. Coastal wetlands. Elsevier, Netherlands, pp 359–381. https://doi.org/10.1016/B978-0-444-63893-9.00010-1

Giannini MB, Parente C (2015) An object based approach for coastline extraction from Quickbird multi-spectral images. Int J Eng Technol 6(6):2698–2704

Giosan L, Syvitski J, Constantinescu S, Day J (2014) Climate change: protect the world's deltas. Nat News 516(7529):31. https://doi.org/10.1038/516031a

Godin OA, Irisov VG, Leben RR, Hamlington BD, Wick GA et al (2009) Variations in sea surface roughness induced by the 2004 Sumatra-Andaman tsunami. Nat Hazards Earth Syst Sci 9:1135–1147. https://doi.org/10.5194/nhess-9-1135-2009

Gomez C, Wulder MA, Dawson AG, Ritchie W, Green DR (2014) Shoreline change and coastal vulnerability characterization with landsat imagery: a case study in the Outer Hebrides, Scotland. Sccotish Geogr J 130:279–299

Gómez-Enri J, Vignudelli S, Quartly GD, Gommenginger CP, Cipollini P, Challenor PG, Benveniste J (2010) Modeling Envisat RA-2 waveforms in the coastal zone: case study of calm water contamination. IEEE Geosci Remote Sens Lett 7(3):474–478. https://doi.org/10.1109/LGRS.2009.2039193

Gong Z, Liang S, Wang X, Pu R (2021) Remote sensing monitoring of the bottom topography in a shallow reservoir and the spatiotemporal changes of submerged aquatic vegetation under water depth fluctuations. IEEE J Sel Top Appl Earth Obs Remote Sens 14:5684–5693. https://doi.org/10.1109/JSTARS.2021.3080692

Gorelick N, Hancher M, Dixon M, Ilyushchenko S, Thau D, Moore R (2017) Google earth engine: planetary-scale geospatial analysis for everyone. Remote Sens Environ 202:18–27. https://doi.org/10.1016/j.rse.2017.06.031

Gouzenes Y, Léger F, Cazenave A, Birol F, Bonnefond P, Passaro M, Nino F, Almar R, Laurain O, Schwatke C, Legeais JF (2020) Coastal sea level rise at Senetosa (Corsica) during the Jason altimetry missions. Ocean Sci 16(5):1165–1182. https://doi.org/10.5194/os-16-1165-2020

Grasso F, Le Hir P (2019) Influence of morphological changes on suspended sediment dynamics in a macrotidal estuary: diachronic analysis in the Seine Estuary (France) from 1960 to 2010. Ocean Dyn 69(1):83–100. https://doi.org/10.1007/s10236-018-1233-x

Guo M, Li J, Sheng C, Xu J, Wu L (2017) A review of wetland remote sensing. Sensors 17(4):777. https://doi.org/10.3390/s17040777

Haigh ID, Eliot M, Pattiaratchi C (2011) Global influences of the 18.61 year nodal cycle and 8.85 year cycle of lunar perigee on high tidal levels. J Geophys Res Ocean. https://doi.org/10.1029/2010JC006645

Hamlington BD, Gardner AS, Ivins E, Lenaerts JT, Reager JT, Trossman DS, Zaron ED, Adhikari S, Arendt A, Aschwanden A, Beckley BD et al (2020) Understanding of contemporary regional sea-level change and the implications for the future. Rev Geophys 58(3):e2019RG000672. https://doi.org/10.1029/2019RG000672

Hamm L, Stive MJF (2002) Shore nourishment in Europe. Coast Eng Spec Issue 47:79–263. https://doi.org/10.1016/S0378-3839(02)00153-9

Han B, Loisel H, Vantrepotte V, Mériaux X, Bryère P, Ouillon S, Dessailly D, Xing Q, Zhu J (2016) Development of a semi-analytical algorithm for the retrieval of suspended particulate matter from remote sensing over clear to very turbid waters. Remote Sens 8(3):211. https://doi.org/10.3390/rs8030211

Hancock S, Armston J, Hofton M, Sun X, Tang H, Duncanson LI, Kellner JR, Dubayah R (2019) The GEDI simulator: a large-footprint waveform lidar simulator for calibration and validation of space-borne missions. Earth Space Sci 6(2):294–310. https://doi.org/10.1029/2018EA000506

Hanssen RF (2001) Radar interferometry: data interpretation and error analysis, vol 2. Springer Science & Business Media, Dordrecht

Harley MDIL, Turner MA, Kinsela JH, Middleton PJ, Mumford KD, Splinter MS, Phillips JA, Simmons DJ, Hanslow AD, Short, (2017) Extreme coastal erosion enhanced by anomalous extratropical storm wave direction. Sci Rep 7:6033

Hemer MA, Fan Y, Mori N, Semedo A, Wang XL (2013) Projected future changes in wind-wave climate in a multi-model ensemble. Nat Clim Chang 3:471–476

Heygster G, Dannenberg J, Notholt J (2009) Topographic mapping of the German tidal flats analyzing SAR images with the waterline method. IEEE Trans Geosci Remote Sens 48(3):1019–1030. https://doi.org/10.1109/TGRS.2009.2031843

Hoeke RK, McInnes KL, Kruger JC, McNaught RJ, Hunter JR, Smithers SG (2013) Widespread inundation of Pacific islands triggered by distant-source wind-waves. Glob Planet Chang 108:128–138

Hoeke RK, McInnes KL, O'Grady JG (2015) Wind and wave setup contributions to extreme sea levels at a tropical high island: a stochastic cyclone simulation study for Apia, Samoa. J Mar Sci Eng 3:1117–1135

Holgate SJ, Matthews A, Woodworth PL, Rickards LJ, Tamisiea ME, Bradshaw E, Foden PR, Gordon KM, Jevrejeva S, Pugh J (2013) New data systems and products at the permanent service for mean sea level. J Coast Res 29(3):493–504. https://doi.org/10.2112/JCOASTRES-D-12-00175.1

Hong SH, Wdowinski S (2013) Multitemporal multitrack monitoring of wetland water levels in the Florida Everglades using ALOS PALSAR data with interferometric processing. IEEE Geosci Remote Sens Lett 11(8):1355–1359

Hongo C, Kurihara H, Golbuu Y (2018) Projecting of wave height and water level on reef-lined coasts due to intensified tropical cyclones and sea level rise in Palau to 2100. Nat Hazards Earth Syst Sci 18:669–686

Hudson AS, Talke SA, Jay DA (2017) Using satellite observations to characterize the response of estuarine turbidity maxima to external forcing. Estuaries Coasts 40(2):343–358. https://doi.org/10.1007/s12237-016-0164-3

Idier D, Bertin X, Thompson P, Pickering MD (2019) Interactions between mean sea level, tide, surge, waves and flooding: mechanisms and contributions to sea level variations at the coast. Surv Geophys 40(6):1603–1630. https://doi.org/10.1007/s10712-019-09549-5

Ikeda M, Dobson F (1995) Oceanographic applications of remote sensing. CRC Press, Boca Raton, p 512

IPCC (2014) Climate change 2014: synthesis report. Contribution of working groups I, II and III to the fifth assessment report of the intergovernmental panel on climate change [Core Writing Team, Pachauri RK, Meyer LA (eds)]. IPCC, Geneva, Switzerland, p 151

IPCC (2019) IPCC special report on the ocean and cryosphere in a changing climate [Pörtner H-O, Roberts DC, Masson-Delmotte V, Zhai P, Tignor M, Poloczanska E, Mintenbeck K, Alegría A, Nicolai M, Okem A, Petzold J, Rama B, Weyer NM (eds)]

IPCC (2021) Climate change 2021: the physical science basis. contribution of working group i to the sixth assessment report of the intergovernmental panel on climate change [Masson-Delmotte V, Zhai P, Pirani A, Connors SL, Péan C, Berger S, Caud N, Chen Y, Goldfarb L, Gomis MI, Huang M, Leitzell K, Lonnoy E, Matthews JBR, Maycock TK, Waterfield T, Yelekçi O, Yu R, Zhou B (eds)]. Cambridge University Press

Jacobs JM, Cattaneo LR, Sweet W, Mansfield T (2018) Recent and future outlooks for nuisance flooding impacts on roadways on the US East Coast. Transp Res Rec 2672(2):1–10. https://doi.org/10.1177/0361198118756366

Jalón-Rojas I, Schmidt S, Sottolichio A (2017) Comparison of environmental forcings affecting suspended sediments variability in two macrotidal, highly-turbid estuaries. Estuar Coast Shelf Sci 198:529–541. https://doi.org/10.1016/j.ecss.2017.02.017

Jawak SD, Vadlamani SS, Luis AJ (2015) A synoptic review on deriving bathymetry information using remote sensing technologies: models, methods and comparisons. Adv Remote Sens 4(02):147. https://doi.org/10.4236/ars.2015.42013

Jay DA, Talke SA, Hudson A, Twardowski M (2015) Estuarine turbidity maxima revisited Instrumental approaches, remote sensing, modeling studies and new directions. In: Ashworth PJ, Best JL, Parsons DR (eds) Developments in sedimentology, vol 68, pp 49–109. https://doi.org/10.1016/B978-0-444-63529-7.00004-3

Jebri F, Birol F, Zakardjian B, Bouffard J, Sammari C (2016) Exploiting coastal altimetry to improve the surface circulation scheme over the central Mediterranean Sea. J Geophys Res Ocean 121(7):4888–4909. https://doi.org/10.1002/2016JC011961

Jiang H, Zheng H, Mu L (2020) Improving altimeter wind speed retrievals using ocean wave parameters. IEEE J Sel Top Appl Earth Obs Remote Sens 13:1917–1924. https://doi.org/10.1109/JSTARS.2020.2993559

Joevivek V, Saravanan S, Chandrasekar N (2013) Coastal vulnerability and shoreline changes for southern tip of India-Remote sensing and GIS approach. J Earth Sci Clim Chang 4:144. https://doi.org/10.4172/2157-7617.1000144

Kang Y, Ding X, Xu F, Zhang C, Ge X (2017) Topographic mapping on large-scale tidal flats with an iterative approach on the waterline method. Estuar Coast Shelf Sci 190:11–22. https://doi.org/10.1016/j.ecss.2017.03.024

Karunarathna H, Horrillo-Caraballo J, Kuriyama Y, Mase H, Ranasinghe R, Reeve DE (2016) Linkages between sediment composition, wave climate and beach profile variability at multiple timescales. Mar Geol 381:194–208

Klein GD (1985) Intertidal flats and intertidal sand bodies. Coastal sedimentary environments. Springer, New York, NY, pp 187–224. https://doi.org/10.1007/978-1-4612-5078-4_3

Kulp SA, Strauss BH (2018) CoastalDEM: a global coastal digital elevation model improved from SRTM using a neural network. Remote Sens Environ 206:231–239. https://doi.org/10.1016/j.rse.2017.12.026

Kumar ED, Sannasiraj SA, Sundar V, Polnikov VG (2013) Wind-wave characteristics and climate variability in the Indian Ocean region using altimeter data. Mar Geod 36(3):303–318. https://doi.org/10.1080/01490419.2013.771718

Kuo CY, Shum CK, Braun A, Mitrovica JX (2004) Vertical crustal motion determined by satellite altimetry and tide gauge data in Fennoscandia. Geophys Res Lett. https://doi.org/10.1029/2003GL019106

Kuriyama Y, Banno M, Suzuki T (2012) Linkages among interannual variations of shoreline, wave and climate at Hasaki, Japon. Geophys Res Lett 39:L06604

Launeau P, Méléder V, Verpoorter C, Barillé L, Kazemipour-Ricci F, Giraud M, Jesus B, Le Menn E (2018) Microphytobenthos biomass and diversity mapping at different spatial scales with a hyperspectral optical model. Remote Sens 10(5):716. https://doi.org/10.3390/rs10050716

Lázaro C, Fernandes MJ, Vieira T, Vieira E (2020) A coastally improved global dataset of wet tropospheric corrections for satellite altimetry. Earth Syst Sci Data 12(4):3205–3228. https://doi.org/10.5194/essd-12-3205-2020

Le Cozannet G, Idier D, de Michele M, Legendre Y, Moisan M, Pedreros R, Thiéblemont R, Spada G, Raucoules D, de la Torre Y (2021) Timescales of emergence of chronic flooding in the major economic center of Guadeloupe. Nat Hazard 21(2):703–722. https://doi.org/10.5194/nhess-21-703-2021

Lee JS, Jurkevich I (1990) Coastline detection and tracing in SAR images. IEEE Trans Geosci Remote Sens 28(4):662–668

Lee SK, Ryu JH (2017) High-accuracy tidal flat digital elevation model construction using TanDEM-X science phase data. IEEE J Sel Top Appl Earth Obs Remote Sens 10(6):2713–2724

Legeais JF, Ablain M, Zawadzki L, Zuo H, Johannessen JA, Scharffenberg MG, Fenoglio-Marc L, Fernandes MJ, Andersen OB, Rudenko S, Cipollini P (2018) An improved and homogeneous altimeter sea level record from the ESA climate change initiative. Earth Syst Sci Data 10(1):281–301. https://doi.org/10.5194/essd-10-281-2018

Lentz EE, Thieler ER, Plant NG, Stippa SR, Horton RM, Gesch DB (2016) Evaluation of dynamic coastal response to sea-level rise modifies inundation likelihood. Nat Clim Chang 6:696–700

Letetrel C, Karpytchev M, Bouin MN, Marcos M, Santamarĺa-Gómez A, Wöppelmann G (2015) Estimation of vertical land movement rates along the coasts of the Gulf of Mexico over the past decades. Cont Shelf Res 111:42–51. https://doi.org/10.1109/TGRS.1990.572976

Leuliette EW, Nerem RS, Mitchum GT (2004) Calibration of TOPEX/Poseidon and Jason altimeter data to construct a continuous record of mean sea level change. Mar Geod 27(1–2):79–94. https://doi.org/10.1080/01490410490465193

Li R, Di K, Ma R (2003) 3-D shoreline extraction from IKONOS satellite imagery. Mar Geod 26(1–2):107–115. https://doi.org/10.1080/01490410306699

Li Z, Heygster G, Notholt J (2014) Intertidal topographic maps and morphological changes in the German Wadden Sea between 1996–1999 and 2006–2009 from the waterline method and SAR images. IEEE J Sel Top Appl Earth Obs Remote Sens 7(8):3210–3224. https://doi.org/10.1109/JSTARS.2014.2313062

Li X, Han G, Yang J, Chen D, Zheng G, Chen N (2018) Using satellite altimetry to calibrate the simulation of typhoon Seth storm surge off Southeast China. Remote Sens 10(4):657. https://doi.org/10.3390/rs10040657

Liao T-H, Simard M, Denbina M, Lamb MP (2020) Monitoring water level change and seasonal vegetation change in the coastal wetlands of louisiana using L-band time-series. Remote Sens 12(15):2351

Lillibridge J, Scharroo R, Abdalla S, Vandemark D (2014) One-and two-dimensional wind speed models for Ka-band altimetry. J Atmos Ocean Technol 31(3):630–638. https://doi.org/10.1175/JTECH-D-13-00167.1

Liu Q, Trinder JC, Turner IL (2017) Automatic super-resolution shoreline change monitoring using Landsat archival data: a case study at Narrabeen-Collaroy Beach, Australia. J Appl Remote Sens 11(1):016036. https://doi.org/10.1117/1.JRS.11.016036

Lobeto H, Menéndez M, Losada IJ (2018) Toward a methodology for estimating coastal extreme sea levels from satellite altimetry. J Geophys Res Ocean 123(11):8284–8298. https://doi.org/10.1029/2018JC014487

Lobeto H, Menéndez M, Losada IJ (2021) Future behavior of wind wave extremes due to climate change. Sci Rep 11(1):1–12. https://doi.org/10.1038/s41598-021-86524-4

Loisel H, Mangin A, Vantrepotte V, Dessailly D, Dinh DN, Garnesson P, Ouillon S, Lefebvre JP, Mériaux X, Phan TM (2014) Variability of suspended particulate matter concentration in coastal waters under the Mekong's influence from ocean color (MERIS) remote sensing over the last decade. Remote Sens Environ 150:218–230. https://doi.org/10.1016/j.rse.2014.05.006

Luijendijk A, Hagenaars G, Ranasinghe R, Baart F, Donchyts G, Aarninkhof S (2018) The state of the world's beaches. Sci Rep 8(1):1–11. https://doi.org/10.1038/s41598-018-24630-6

Lyzenga DR (1978) Passive remote sensing techniques for mapping water depth and bottom features. Appl Opt 17(3):379–383. https://doi.org/10.1364/AO.17.000379

Markus T, Neumann T, Martino A, Abdalati W, Brunt K, Csatho B, Farrell S, Fricker H, Gardner A, Harding D, Jasinski M (2017) The ice, cloud, and land elevation Satellite-2 (ICESat-2): science requirements, concept, and implementation. Remote Sens Environ 190:260–273. https://doi.org/10.1016/j.rse.2016.12.029

Marti F, Cazenave A, Birol F, Passaro M, Léger F, Niño F, Almar R, Benveniste J, Legeais JF (2021) Altimetry-based sea level trends along the coasts of western Africa. Adv Space Res 68(2):504–522. https://doi.org/10.1016/j.asr.2019.05.033

Mason DC, Davenport IJ, Robinson GJ, Flather RA, McCartney BS (1995) Construction of an inter-tidal digital elevation model by the 'Water-Line'Method. Geophys Res Lett 22(23):3187–3190. https://doi.org/10.1029/95GL03168

Mathers EL, Woodworth PL (2001) Departures from the local inverse barometer model observed in altimeter and tide gauge data and in a global barotropic numerical model. J Geophys Res Ocean 106(C4):6957–6972

Mayer L, Jakobsson M, Allen G, Dorschel B, Falconer R, Ferrini V (2018) The nippon foundation - GEBCO seabed 2030 project: the quest to see the world's oceans completely mapped by 2030. Geosciences 8:63. https://doi.org/10.3390/geosciences8020063

Mc Carthy BL (2010) Coastal bathymetry using satellite observation in support of intelligence preparation of the environment, Calhoun thesis: The NPS Institutional Archive DSpace Repository

McFeeters SK (1996) The use of the normalized difference water index (NDWI) in the delineation of open water features. Int J Remote Sens 17(7):1425–1432. https://doi.org/10.1080/01431169608948714

McKenzie LJ, Nordlund LM, Jones BL, Cullen-Unsworth LC, Roelfsema C, Unsworth RK (2020) The global distribution of seagrass meadows. Environ Res Lett 15(7):074041. https://doi.org/10.1088/1748-9326/ab7d06

Mcowen CJ, Weatherdon LV, Van Bochove JW, Sullivan E, Blyth S, Zockler C, Stanwell-Smith D, Kingston N, Martin CS, Spalding M, Fletcher S (2017) A global map of saltmarshes. Biodivers Data J. https://doi.org/10.3897/BDJ.5.e11764

Melet A, Almar R, Meyssignac B (2016) What dominates sea level at the coast: a case study for the Gulf of Guinea. Ocean Dyn 66:623–636

Melet A, Meyssignac B, Almar R, Le Cozannet G (2018) Under-estimated wave contribution to coastal sea-level rise. Nat Clim Chang 8(3):234–239. https://doi.org/10.1038/s41558-018-0088-y

Melet A, Teatini P, Le Cozannet G, Jamet C, Conversi A, Benveniste J, Almar R (2020) Earth observations for monitoring marine coastal hazards and their drivers. Surv Geophys 41(6):1489–1534. https://doi.org/10.1007/s10712-020-09594-5

Menéndez M, Woodworth PL (2010) Changes in extreme high water levels based on a quasi-global tide-gauge data set. J Geophys Res Ocean. https://doi.org/10.1029/2009JC005997

Mentaschi L, Vousdoukas MI, Voukouvalas E, Dosio A, Feyen L (2017) Global changes of extreme coastal wave energy fluxes triggered by intensified teleconnection patterns. Geophys Res Lett 44:2416–2426

Mentaschi L, Vousdoukas MI, Pekel JF, Voukouvalas E, Feyen L (2018) Global long-term observations of coastal erosion and accretion. Sci Rep 8(1):1–11. https://doi.org/10.1038/s41598-018-30904-w

Menuge B, Verpoorter C, Héquette A, Sipka V (2020) Mapping of estuarine transport from spatial remote-sensing products: application to Authie Bay (France). Estuaries and coastal zones in times of global change. Springer, Singapore, pp 809–830. https://doi.org/10.1007/978-981-15-2081-5_47

Merrifield M, Kilonsky B, Nakahara S (1999) Interannual sea level changes in the tropical Pacific associated with ENSO. Geophys Res Lett 26(21):3317–3320. https://doi.org/10.1029/1999GL010485

Minderhoud PSJ, Coumou L, Erban LE, Middelkoop H, Stouthamer E, Addink EA (2018) The relation between land use and subsidence in the Vietnamese Mekong delta. Sci Total Environ 634:715–726. https://doi.org/10.1016/j.scitotenv.2018.03.372

Minderhoud PSJ, Middelkoop H, Erkens G, Stouthamer E (2020) Groundwater extraction may drown mega-delta: projections of extraction-induced subsidence and elevation of the Mekong delta for the 21st century. Environ Res Commun 2(1):011005. https://doi.org/10.1088/2515-7620/ab5e21

Monteys X, Harris P, Caloca S, Cahalane C (2015) Spatial prediction of coastal bathymetry based on mul-
    tispectral satellite imagery and multibeam data. Remote Sens 7(10):13782–13806. https://doi.org/10.
    3390/rs71013782
Mori N, Shimura T, Yoshida K, Mizuta R, Okada Y, Fujita M, Khujanazarov T, Nakakita E (2019) Future
    changes in extreme storm surges based on mega-ensemble projection using 60-km resolution atmos-
    pheric global circulation model. Coast Eng J 61(3):295–307. https://doi.org/10.1080/21664250.2019.
    1586290
Morim J, Hemer MA, Cartwright N, Strauss D, Andutta F (2018) On the concordance of 21st century wind-
    wave climate projections. Glob Planet Chang 167:160–171
Morim J, Hemer M, Wang XL, Cartwright N, Trenham C, Semedo A, Young I, Brichero L, Camus P,
    Casas-Prat M, Erikson L et al (2019) Robustness and uncertainties in global multivariate wind-wave
    climate projections. Nat Clim Chang 9:711–718
Morim J, Vitousek S, Hemer M, Reguero B, Erikson L, Casas-Prat M, Wang XL, Semedo A, Mori N,
    Shimura T, Mentaschi L (2021) Global-scale changes to extreme ocean wave events due to anthropo-
    genic warming. Environ Res Lett 16(7):074056. https://doi.org/10.1088/1748-9326/ac1013
Morrow R, Fu LL, Ardhuin F, Benkiran M, Chapron B, Cosme E, d'Ovidio F, Farrar JT, Gille ST, Lapeyre
    G, Le Traon PY (2019) Global observations of fine-scale ocean surface topography with the surface
    water and ocean topography (SWOT) mission. Front Mar Sci 6:232. https://doi.org/10.3389/fmars.
    2019.00232
Mouyen M, Longuevergne L, Steere P, Crave A, Lemoine JM, Himanshu S, Robin C (2018) Assessing mod-
    ern river sediment discharge to the ocean using satellite gravimetry. Source to sink: a long term per-
    spective of sediment budgets and sources characterization, Géosciences-Rennes, Nov 2016, Rennes,
    France. p 79. ⟨insu-01406500⟩
Muis S, Haigh ID, Guimarães Nobre G, Aerts JC, Ward PJ (2018) Influence of El Niño-Southern Oscillation
    on global coastal flooding. Earth's Future 6(9):1311–1322. https://doi.org/10.1029/2018EF000909
Muis S, Irazoqui Apecechea M, Dullaart J, Yan K, De Lima Rego J, Su J, Madsen KS, Verlaan M (2020)
    CoDEC Dataset - Data underlying the paper "A high-resolution global dataset of extreme sea levels,
    tides and storm surges including future projections ". Front Mar Sci
Murray NJ, Phinn SR, DeWitt M, Ferrari R, Johnston R, Lyons MB, Clinton N, Thau D, Fuller RA (2019)
    The global distribution and trajectory of tidal flats. Nature 565(7738):222–225. https://doi.org/10.
    1038/s41586-018-0805-8
Nechad B, Ruddick KG, Park Y (2010) Calibration and validation of a generic multisensor algorithm for
    mapping of total suspended matter in turbid waters. Remote Sens Environ 114(4):854–866. https://
    doi.org/10.1016/j.rse.2009.11.022
Nerem RS, Mitchum GT (2001) Sea level change. In: International geophysics, Academic Press, vol 69, pp
    329-xxiii. https://doi.org/10.1016/S0074-6142(01)80153-4
Neumann B, Vafeidis AT, Zimmermann J, Nicholls RJ (2015) Future coastal population growth and expo-
    sure to sea-level rise and coastalflooding - a global assessment. PLoS ONE 10(3):e0118571. https://
    doi.org/10.1371/journal.pone.0118571
Ngoc DD, Loisel H, Vantrepotte V, Chu Xuan H, Nguyen Minh N, Verpoorter C, Meriaux X, Pham Thi
    Minh H, Le Thi H, Le Vu Hong H, Van Nguyen T (2020) A simple empirical band-ratio algorithm to
    assess suspended particulate matter from remote sensing over coastal and inland waters of Vietnam:
    application to the VNREDSat-1/NAOMI sensor. Water 12(9):2636. https://doi.org/10.3390/w1209
    2636
Nicholls RJ, Lincke D, Hinkel J, Brown S, Vafeidis AT, Meyssignac B, Hanson SE, Merkens JL, Fang J
    (2021) A global analysis of subsidence, relative sea-level change and coastal flood exposure. Nat
    Clim Chang 11(4):338–342. https://doi.org/10.1038/s41558-021-00993-z
Nienhuis JH, Ashton AD, Edmonds DA, Hoitink AJF, Kettner AJ, Rowland JC, Törnqvist TE (2020) Global-
    scale human impact on delta morphology has led to net land area gain. Nature 577(7791):514–518.
    https://doi.org/10.1038/s41586-019-1905-9
Norcross ZM, Fletcher CH, Merrifield M (2002) Annual and interannual changes on a reef-fringed pocket
    beach: Kailua Bay, Hawaii. Mar Geol 190:553–580
Normandin C, Lubac B, Sottolichio A, Frappart F, Ygorra B, Marieu V (2019) Analysis of suspended sedi-
    ment variability in a large highly turbid estuary using a 5-year-long remotely sensed data archive
    at high resolution. J Geophys Res Ocean 124(11):7661–7682. https://doi.org/10.1029/2019JC015417
Novoa S, Doxaran D, Ody A, Vanhellemont Q, Lafon V, Lubac B, Gernez P (2017) Atmospheric correc-
    tions and multi-conditional algorithm for multi-sensor remote sensing of suspended particulate mat-
    ter in low-to-high turbidity levels coastal waters. Remote Sens 9(1):61. https://doi.org/10.3390/rs901
    0061

O'Grady J, McInnes KL, Hemer MA, Hoeke R, Stephenson A, Colberg F (2019) Extreme water levels for Australian beaches using empirical equations for shoreline wave setup. JGR-Ocean 124(8):5468–5484

OECD (2005) OECD annual report, 45th anniversary, p 147

Ostanciaux E, Husson L, Choblet G, Robin C, Pedoja K (2012) Present-day trends of vertical ground motion along the coast lines. Earth Sci Rev 110(1–4):74–92. https://doi.org/10.1016/j.earscirev.2011.10.004

Pardo-Pascual JE, Almonacid-Caballer J, Ruiz LA, Palomar-Vázquez J (2012) Automatic extraction of shorelines from Landsat TM and ETM+ multi-temporal images with subpixel precision. Remote Sens Environ 123:1–11. https://doi.org/10.1016/j.rse.2012.02.024

Pascual A, Lana A, Troupin C, Ruiz S, Faugère Y, Escudier R, Tintoré J (2015) Assessing SARAL/AltiKa data in the coastal zone: comparisons with HF radar observations. Mar Geod 38(sup1):260–276. https://doi.org/10.1080/01490419.2015.1019656

Passaro M, Cipollini P, Vignudelli S, Quartly GD, Snaith HM (2014) ALES: a multi-mission adaptive subwaveform retracker for coastal and open ocean altimetry. Remote Sens Environ 145:173–189. https://doi.org/10.1016/j.rse.2014.02.008

Passaro M, Cipollini P, Benveniste J (2015) Annual sea level variability of the coastal ocean: the Baltic Sea-North Sea transition zone. J Geophys Res Ocean 120(4):3061–3078. https://doi.org/10.1002/2014JC010510

Passaro M, Dinardo S, Quartly GD, Snaith HM, Benveniste J, Cipollini P, Lucas B (2016) Cross-calibrating ALES Envisat and CryoSat-2 Delay–Doppler: a coastal altimetry study in the Indonesian Seas. Adv Space Res 58(3):289–303. https://doi.org/10.1016/j.asr.2016.04.011

Passaro M, Hemer MA, Quartly GD, Schwatke C, Dettmering D, Seitz F (2021) Global coastal attenuation of wind-waves observed with radar altimetry. Nat Commun 12(1):1–13. https://doi.org/10.1038/s41467-021-23982-4

Pedreros R, Idier D, Muller H, Lecacheux S, Paris F, Yates-Michelin M, Dumas F, Pineau-Guillou L, Senechal N (2018) Relative contribution of wave setup to the storm surge: observations and modeling based analysis in open and protected environments (Truc Vert beach and Tubuai island). J Coast Res 85(10085):1046–1050. https://doi.org/10.2112/SI85-210.1

Peng D, Hill EM, Meltzner AJ, Switzer AD (2019) Tide gauge records show that the 18.61-year nodal tidal cycle can change high water levels by up to 30 cm. J Geophys Res Ocean 124(1):736–749. https://doi.org/10.1029/2018JC014695

Pfeffer J, Allemand P (2016) The key role of vertical land motions in coastal sea level variations: a global synthesis of multisatellite altimetry, tide gauge data and GPS measurements. Earth Planet Sci Lett 439:39–47. https://doi.org/10.1016/j.epsl.2016.01.027

Piccioni G, Dettmering D, Passaro M, Schwatke C, Bosch W, Seitz F (2018) Coastal improvements for tide models: the impact of ALES retracker. Remote Sens 10(5):700. https://doi.org/10.3390/rs10050700

Pleskachevsky A, Lehner S, Heege T, Mott C (2011) Synergy and fusion of optical and synthetic aperture radar satellite data for underwater topography estimation in coastal areas. Ocean Dyn 61(12):2099–2120. https://doi.org/10.1007/s10236-011-0460-1

Ponte RM, Carson M, Cirano M, Domingues CM, Jevrejeva S, Marcos M, Mitchum G, van de Wal RSW, Woodworth PL, Ablain M, Ardhuin F, Ballu V, Becker M, Benveniste J, Birol F, Bradshaw E, Cazenave A, de Mey-Frémaux P, Durand F, Ezer T, Fu LL, Fukumori I, Gordon K, Gravelle M, Griffies SM, Han W, Hibbert A, Hughes CW, Idier D, Kourafalou VH, Little CM, Matthews A, Melet A, Merrifield M, Meyssignac B, Minobe S, Penduff T, Picot N, Piecuch C, Ray RD, Rickards L, Santamaría-Gómez A, Stammer D, Staneva J, Testut L, Thompson K, Thompson P, Vignudelli S, Williams J, Williams SDP, Wöppelmann G, Zanna L, Zhang X (2019) Towards comprehensive observing and modeling systems for monitoring and predicting regional to coastal sea level. Front Mar Sci 6:437. https://doi.org/10.3389/fmars.2019.00437

Poupardin A, Idier D, de Michele M, Raucoules D (2015) Water depth inversion from a single SPOT-5 dataset. IEEE Trans Geosci Remote Sens 54(4):2329–2342. https://doi.org/10.1109/TGRS.2015.2499379

Pugh DT (1996) Tides, surges and mean sea-level (reprinted with corrections), Wiley, Chichester, UK, pp. 486

Pugh D (2004) Changing sea levels: effects of tides, weather and climate. Cambridge University Press

Pujol MI, Faugère Y, Taburet G, Dupuy S, Pelloquin C, Ablain M, Picot N (2016) DUACS DT2014: the new multi-mission altimeter data set reprocessed over 20 years. Ocean Sci 12(5):1067–1090. https://doi.org/10.5194/os-12-1067-2016

Quilfen Y, Yurovskaya M, Chapron B, Ardhuin F (2018) Storm waves focusing and steepening in the Agulhas current: Satellite T observations and modeling. Remote Sens Environ 216:561–571. https://doi.org/10.1016/j.rse.2018.07.020

Radenac MH, Léger F, Messié M, Dutrieux P, Menkes C, Eldin G (2016) Wind-driven changes of surface current, temperature, and chlorophyll observed by satellites north of New Guinea. J Geophys Res Ocean 121(4):2231–2252. https://doi.org/10.1002/2015JC011438

Rasquin C, Seiffert R, Wachler B, Winkel N (2020) The significance of coastal bathymetry representation for modelling the tidal response to mean sea level rise in the German Bight. Ocean Sci 16(1):31–44

Rateb A, Abotalib AZ (2020) Inferencing the land subsidence in the Nile Delta using Sentinel-1 satellites and GPS between 2015 and 2019. Sci Total Environ 729:138868. https://doi.org/10.1016/j.scitotenv.2020.138868

Raucoules D, Le Cozannet G, Wöppelmann G, De Michele M, Gravelle M, Daag A, Marcos M (2013) High nonlinear urban ground motion in Manila (Philippines) from 1993 to 2010 observed by DInSAR: implications for sea-level measurement. Remote Sens Environ 139:386–397. https://doi.org/10.5194/os-16-31-2020

Ray RD, Zaron ED (2011) Non-stationary internal tides observed with satellite altimetry. Geophys Res Lett. https://doi.org/10.1029/2011GL048617

Reguero BG, Losada IJ, Méndez FJ (2019) A recent increase in global wave power as a consequence of oceanic warming. Nat Commun 10(1):205. https://doi.org/10.1038/s41467-018-08066-0

Ribal A, Young IR (2019) 33 years of globally calibrated wave height and wind speed data based on altimeter observations. Sci Data 6(1):1–15. https://doi.org/10.1038/s41597-019-0083-9

Riethmüller R, Heineke M, Kühl H, Keuker-Rüdiger R (2000) Chlorophyll a concentration as an index of sediment surface stabilisation by microphytobenthos? Cont Shelf Res 20(10–11):1351–1372. https://doi.org/10.1016/S0278-4343(00)00027-3

Rizzoli P, Martone M, Gonzalez C, Wecklich C, Tridon DB, Bräutigam B, Bachmann M, Schulze D, Fritz T, Huber M, Wessel B (2017) Generation and performance assessment of the global TanDEM-X digital elevation model. ISPRS J Photogramm Remote Sens 132:119–139. https://doi.org/10.1016/j.isprsjprs.2017.08.008

Rodolfo KS, Siringan FP (2006) Global sea-level rise is recognised, but flooding from anthropogenic land subsidence is ignored around northern Manila Bay, Philippines. Disasters 30(1):118–139. https://doi.org/10.1111/j.1467-9523.2006.00310.x

Rowan GSL, Kalacska M (2021) A review of remote sensing of submerged aquatic vegetation for non-specialists. Remote Sens 13(4):623

Rueda A, Vitousek S, Camus P, Tomas A, Epejo A, Losada IJ, Barnard P, Erikson L, Ruggiero P, Reguero BG, Mendez FJ (2017) Global classification of coastal flooding climates. Sci Rep 7(1):5038. https://doi.org/10.1038/s41598-017-05090-w

Ruggiero P (2013) Is the intensifying wave climate of the U.S. Pacific Northwest increasing flooding and erosion risk faster than sea level rise? J Waterw Port Coast Ocean Eng 139(2):88–97. https://doi.org/10.1061/(ASCE)WW.1943-5460.0000172

Rundquist DC, Lawson MP, Queen LP, Cerveny RS (1987) The relationship between summer-season rainfall events and lake-surface area. JAWRA J Am Water Resour Assoc 23(3):493–508. https://doi.org/10.1111/j.1752-1688.1987.tb00828.x

Ryu JH, Kim CH, Lee YK, Won JS, Chun SS, Lee S (2008) Detecting the intertidal morphologic change using satellite data. Estuar Coast Shelf Sci 78(4):623–632. https://doi.org/10.1016/j.ecss.2008.01.020

Sagawa T, Yamashita Y, Okumura T, Yamanokuchi T (2019) Satellite derived bathymetry using machine learning and multi-temporal satellite images. Remote Sens 11(10):1155. https://doi.org/10.3390/rs11101155

Salameh E, Frappart F, Marieu V, Spodar A, Parisot JP, Hanquiez V, Turki I, Laignel B (2018) Monitoring sea level and topography of coastal lagoons using satellite radar altimetry: the example of the Arcachon Bay in the Bay of Biscay. Remote Sens 10(2):297. https://doi.org/10.3390/rs10020297

Salameh E, Frappart F, Almar R, Baptista P, Heygster G, Lubac B, Raucoules D, Almeida LP, Bergsma EW, Capo S, De Michele M (2019) Monitoring beach topography and nearshore bathymetry using spaceborne remote sensing: a review. Remote Sens 11(19):2212. https://doi.org/10.3390/rs11192212

Salameh E, Frappart F, Turki I, Laignel B (2020) Intertidal topography mapping using the waterline method from Sentinel-1 & -2 images: the examples of Arcachon and Veys Bays in France. ISPRS J Photogramm Remote Sens 163:98–120. https://doi.org/10.1016/j.isprsjprs.2020.03.003

Salameh E, Frappart F, Desroches D, Turki I, Carbonne D, Laignel B (2021) Monitoring intertidal topography using the future SWOT (surface water and ocean topography) mission. Remote Sens Appl Soc Environ 23:100578. https://doi.org/10.1016/j.rsase.2021.100578

Salazar-Ceciliano J, Trasviña-Castro A, González-Rodríguez E (2018) Coastal currents in the Eastern Gulf of Tehuantepec from coastal altimetry. Adv Space Res 62(4):866–873. https://doi.org/10.1016/j.asr.2018.05.033

Santamaría-Gómez A, Gravelle M, Wöppelmann G (2014) Long-term vertical land motion from double-differenced tide gauge and satellite altimetry data. J Geod 88(3):207–222. https://doi.org/10.1007/s00190-013-0677-5

Santamaría-Gómez A, Gravelle M, Dangendorf S, Marcos M, Spada G, Wöppelmann G (2017) Uncertainty of the 20th century sea-level rise due to vertical land motion errors. Earth Planet Sci Lett 473:24–32. https://doi.org/10.1016/j.epsl.2017.05.038

Stammer D, Cazenave A (eds) (2018) Satellite altimetry over oceans and land surfaces. CRC Press, Taylor & Francis, p 620. ISBN 978-1-4987-4345

Scagliola M (2013) CryoSat footprints. Tech Rep 1.2, Aresys

Scharroo R, Bonekamp H, Ponsard C, Parisot F, von Engeln A, Tahtadjiev M, de Vriendt K, Montagner F (2016) Jason continuity of services: continuing the Jason altimeter data records as Copernicus Sentinel-6. Ocean Sci. https://doi.org/10.5194/os-12-471-2016

Semedo A, Suselj K, Rutgersson A, Sterl A (2011) A global view on the wind sea and swell climate and variability from ERA-40. J Clim 24(5):1461–1479. https://doi.org/10.1175/2010JCLI3718.1

Senechal N, Coco G, Bryan KR, Holman RA (2011) Wave runup during extreme storm conditions. J Geophys Res Ocean 116:C07032. https://doi.org/10.1029/2010JC006819

Serafin KA, Ruggiero P, Barnard PL, Stockdon HF (2019) The influence of shelf bathymetry and beach topography on extreme total water levels: linking large-scale changes of the wave climate to local coastal hazards. Coast Eng 150:1–17. https://doi.org/10.1016/j.coastaleng.2019.03.012

Shirzaei M, Freymueller J, Törnqvist TE, Galloway DL, Dura T, Minderhoud PS (2021) Measuring, modelling and projecting coastal land subsidence. Nat Rev Earth Environ 2(1):40–58. https://doi.org/10.1038/s43017-020-00115-x

Siddiqui MN, Maajid S (2004) Monitoring of geomorphological changes for planning reclamation work in coastal area of Karachi, Pakistan. Adv Space Res 33(7):1200–1205. https://doi.org/10.1016/S0273-1177(03)00373-9

Simard M, Fatoyinbo L, Smetanka C, Rivera-Monroy VH, Castañeda-Moya E, Thomas N, Van der Stocken T (2019) Mangrove canopy height globally related to precipitation, temperature and cyclone frequency. Nat Geosci 12(1):40–45. https://doi.org/10.1038/s41561-018-0279-1

Small C, Nicholls RJ (2003) A global analysis of human settlement in coastal zones. J Coast Res 19(3):584–599

Stal LJ (2010) Microphytobenthos as a biogeomorphological force in intertidal sediment stabilization. Ecol Eng 36(2):236–245. https://doi.org/10.1016/j.ecoleng.2008.12.032

Stammer D, Cazenave A, Ponte RM, Tamisiea ME (2013) Causes for contemporary regional sea level-changes. Ann Rev Marine Sci 5:21–46

Stockdon HF, Holman RA, Howd PA, Sallenger AH (2006) Empirical parameterization of setup, swash, and runup. Coast Eng 53(7):573–588. https://doi.org/10.1016/j.coastaleng.2005.12.005

Sweet WV, Park J (2014) From the extreme to the mean: acceleration and tipping points of coastal inundation from sea level rise. Earth's Future 2(12):579–600. https://doi.org/10.1002/2014EF000272

Syvitski JP, Kettner AJ, Overeem I, Hutton EW, Hannon MT, Brakenridge GR, Day J, Vörösmarty C, Saito Y, Giosan L, Nicholls RJ (2009) Sinking deltas due to human activities. Nat Geosci 2(10):681–686. https://doi.org/10.1038/ngeo629

Tadono T, Nagai H, Ishida H, Oda F, Naito S, Minakawa K, Iwamoto H (2016) Generation of the 30-m mesh global digital surface model by ALOS PRISM. Int Arch Photogramm Remote Sens Spat Inf Sci XLI-B4:157–162. https://doi.org/10.5194/isprsarchives-XLI-B4-157-2016

Tateishi R, Akutsu A (1992) Relative DEM production from SPOT data without GCP. Int J Remote Sens 13(14):2517–2530. https://doi.org/10.1080/01431169208904061

Taveneau A, Almar R, Bergsma EW, Sy BA, Ndour A, Sadio M, Garlan T (2021) Observing and predicting coastal erosion at the Langue de Barbarie sand spit around Saint Louis (Senegal, West Africa) through satellite-derived digital elevation model and shoreline. Remote Sens 13(13):2454. https://doi.org/10.3390/rs13132454

Tessler ZD, Vörösmarty CJ, Grossberg M, Gladkova I, Aizenman H (2016) A global empirical typology of anthropogenic drivers of environmental change in deltas. Sustain Sci 11:525–537

Thomas N, Simard M, Castañeda-Moya E, Byrd K, Windham-Myers L, Bevington A, Twilley RR (2019) High-resolution mapping of biomass and distribution of marsh and forested wetlands in southeastern coastal Louisiana. Int J Appl Earth Obs Geoinf 80:257–267. https://doi.org/10.1016/j.jag.2019.03.013

Thomas N, Pertiwi AP, Traganos D, Lagomasino D, Poursanidis D, Moreno S, Fatoyinbo L (2021) Space-borne cloud-native satellite-derived bathymetry (SDB) models using ICESat-2 and Sentinel-2? Geophys Res Lett. https://doi.org/10.1029/2020GL092170

Toimil A, Losada IJ, Nicholls RJ, Dalrymple RA, Stive MJ (2020) Addressing the challenges of climate change risks and adaptation in coastal areas: a review. Coast Eng 156:103611. https://doi.org/10.1016/j.coastaleng.2019.103611

Toure S, Diop O, Kpalma K, Maiga AS (2019) Shoreline detection using optical remote sensing: a review. ISPRS Int J Geo-Inf 8(2):75. https://doi.org/10.3390/ijgi8020075

Tran N, Vandemark D, Labroue S, Feng H, Chapron B, Tolman HL, Lambin J, Picot N (2010) Sea state bias in altimeter sea level estimates determined by combining wave model and satellite data. J Geophys Res Ocean. https://doi.org/10.1029/2009JC005534

Tseng KH, Kuo CY, Lin TH, Huang ZC, Lin YC, Liao WH, Chen CF (2017) Reconstruction of time-varying tidal flat topography using optical remote sensing imageries. ISPRS J Photogramm Remote Sens 131:92–103. https://doi.org/10.1016/j.isprsjprs.2017.07.008

Tucker CJ, Sellers PJ (1986) Satellite remote sensing of primary production. Int J Remote Sens 7(11):1395–1416. https://doi.org/10.1080/01431168608948944

Uncles RJ, Stephens JA, Harris C (2006) Runoff and tidal influences on the estuarine turbidity maximum of a highly turbid system: the upper Humber and Ouse Estuary, UK. Mar Geol 235(1–4):213–228. https://doi.org/10.1016/j.margeo.2006.10.015

UNEP-WCMC (2021) Global distribution of seagrasses (version 7.1). Seventh update to the data layer used in Green and Short (2003). UN Environment World Conservation Monitoring Centre. Data, Cambridge (UK). https://doi.org/10.34892/x6r3-d211

Valiela I (2006) Global coastal change. Blackwell, Oxford, p 368

Vandebroek E, Lindenbergh R, Van Leijen F, De Schipper M, De Vries S, Hanssen R (2017) Semi-automated monitoring of a mega-scale beach nourishment using high-resolution terrasar-x satellite data. Remote Sens 9(7):653. https://doi.org/10.3390/rs9070653

Verpoorter C, Carrère V, Combe JP (2014) Visible, near-infrared spectrometry for simultaneous assessment of geophysical sediment properties (water and grain size) using the spectral derivative-modified Gaussian model. J Geophys Res Earth Surf 119(10):2098–2122. https://doi.org/10.1002/2013JF002969

Verpoorter C, Menuge B, Launeau P, Méléder V, Héquette A, Cartier A, Sipka V (2020) Synergy between hyperspectral (HYSPEX), multispectral (SPOT 6/7, Sentinel-2) remotely sensed data and LiDAR data for mapping the Authie estuarie (France). Estuaries and coastal zones in times of global change. Springer, Singapore, pp 769–788. https://doi.org/10.1007/978-981-15-2081-5_45

Vignudelli S, Cipollini P, Roblou L, Lyard F, Gasparini GP, Manzella G, Astraldi M (2005) Improved satellite altimetry in coastal systems: case study of the Corsica Channel (Mediterranean Sea). Geophys Res Lett. https://doi.org/10.1029/2005GL022602

Vignudelli S, Kostianoy AG, Cipollini P, Benveniste J (eds) (2011) Coastal altimetry. Springer Science & Business Media, Berlin, p 565. https://doi.org/10.1007/978-3-642-12796-0

Vignudelli S, Birol F, Benveniste J, Fu LL, Picot N, Raynal M, Roinard H (2019) Satellite altimetry measurements of sea level in the coastal zone. Surv Geophys 40(6):1319–1349. https://doi.org/10.1007/s10712-019-09569-1

Vinogradov SV, Ponte RM (2010) Annual cycle in coastal sea level from tide gauges and altimetry. J Geophys Res Ocean. https://doi.org/10.1029/2009JC005767

Vitousek S, Barnard PL, Fletcher CH, Frazer N, Erikson L, Storlazzi CD (2017) Doubling of coastal flooding frequency within decades due to sea-level rise. Nature 7:1399

Vos K, Harley MD, Splinter KD, Simmons JA, Turner IL (2019a) Sub-annual to multi-decadal shoreline variability from publicly available satellite imagery. Coast Eng 150:160–174. https://doi.org/10.1016/j.coastaleng.2019.04.004

Vos K, Splinter KD, Harley MD, Simmons JA, Turner IL (2019b) CoastSat: a google earth engine-enabled python toolkit to extract shorelines from publicly available satellite imagery. Environ Model Softw 122:104528. https://doi.org/10.1016/j.envsoft.2019.104528

Vos K, Harley MD, Splinter KD, Walker A, Turner IL (2020) Beach slopes from satellite-derived shorelines. Geophys Res Lett 47(14):e2020GL088365. https://doi.org/10.1029/2020GL088365

Vousdoukas MI, Voukouvalas E, Mentaschi L, Dottori F, Giardino A, Bouziotas D, Bianchi A, Salamon P, Feyen L (2016) Developments in large-scale coastal flood hazard mapping. Nat Hazard 16(8):1841–1853. https://doi.org/10.5194/nhess-16-1841-2016

Vousdoukas MI, Mentaschi L, Voukouvalas E, Verlaan M, Feyen L (2017) Extreme sea levels on the rise along Europe's coasts. Earth's Future 5(3):304–323. https://doi.org/10.1002/2016EF000505

Vousdoukas MI, Mentaschi L, Voukouvalas E, Bianchi A, Dottori F, Feyen L (2018a) Climatic and socio-economic controls of future coastal flood risk in Europe. Nat Clim Chang 8(9):776–780. https://doi.org/10.1038/s41558-018-0260-4

Vousdoukas MI, Mentaschi L, Voukouvalas E, Verlaan M, Jevrejeva S, Jackson LP, Feyen L (2018b) Global probabilistic projections of extreme sea levels show intensification of coastal flood hazard. Nat Commun 9(1):2360. https://doi.org/10.1038/s41467-018-04692-w

Vousdoukas MI, Ranasinghe R, Mentaschi L, Plomaritis TA, Panagiotis A, Arjen L, Feyen L (2020) Sandy coastline under threat of erosion. Nat Clim Chang Lett 10:260–263. https://doi.org/10.1038/s41558-020-0697-0

Wadey M, Brown S, Nicholls RJ, Haigh I (2017) Coastal flooding in the Maldives: an assessment of historic events and their implications. Nat Hazards 89(1):131–159. https://doi.org/10.1007/s11069-017-2957-5

Wahl T, Haigh ID, Nicholls RJ, Arns A, Dangendorf S, Hinkel J, Slangen ABA (2017) Understanding extreme sea levels for broad-scale coastal impact and adaptation analysis. Nat Commun 8(1):16,075. https://doi.org/10.1038/ncomms16075

Wandres M, Pattiaratchi C, Hemer MA (2017) Projected changes of the southwest Australian wave climate under two atmospheric greenhouse gas concentration pathways. Ocean Model 117:70–87. https://doi.org/10.1016/j.ocemod.2017.08.002

Wang XL, Feng Y, Swail VR (2014) Changes in global ocean wave heights as projected using multimodel CMIP5 simulations. Geophys Res Lett 41:1026–1034. https://doi.org/10.1002/2013GL058650

Wdowinski S, Kim S-W, Amelung F, Dixon TH, Miralles-Wilhelm F, Sonenshein R (2008) Space-based detection of wetlands' surface water level changes from L-band SAR interferometry. Remote Sens Environ 112(3):681–696

Williams J, Horsburgh KJ, Williams JA, Proctor RN (2016) Tide and skew surge independence: new insights for flood risk. Geophys Res Lett 43(12):6410–6417

Wölfl AC, Snaith H, Amirebrahimi S, Devey CW, Dorschel B, Ferrini V, Huvenne VA, Jakobsson M, Jencks J, Johnston G, Lamarche G (2019) Seafloor mapping–the challenge of a truly global ocean bathymetry. Front Mar Sci. https://doi.org/10.3389/fmars.2019.00283

Won JS, Kim SW (2003) ERS SAR interferometry for tidal flat DEM. In: Proc. of FRINGE 2003 workshop, Frascati, Italy

Woodworth PL, Hunter JR, Marcos M, Caldwell P, Menéndez M, Haigh I (2016) Towards a global higher-frequency sea level dataset. Geosci Data J 3(2):50–59. https://doi.org/10.1002/gdj3.42

Woodworth PL, Melet A, Marcos M, Ray RD, Wöppelmann G, Sasaki YN, Cirano M, Hibbert A, Huthnance JM, Monserrat S, Merrifield MA (2019) Forcing factors affecting sea level changes at the coast. Surv Geophys 40(6):1351–1397. https://doi.org/10.1007/s10712-019-09531-1

Wöppelmann G, Marcos M (2016) Vertical land motion as a key to understanding sea level change and variability. Rev Geophys 54(1):64–92. https://doi.org/10.1002/2015RG000502

Work EA, Gilmer DS (1976) Utilization of satellite data for inventorying prairie ponds and lakes. Photogramm Eng Remote Sens 42(5):685–694

Wright HL, Pilkey OH (1989) The effect of hard stabilization upon dry beach width. In: Coastal zone'89, ASCE, pp 776–790

Young IR, Ribal A (2019) Multiplatform evaluation of global trends in wind speed and wave height. Science 364(6440):548–552. https://doi.org/10.1126/science.aav9527

Young IR, Vinoth J (2013) An "extended fetch" model for the spatial distribution of tropical cyclone wind–waves as observed by altimeter. Ocean Eng 70:14–24. https://doi.org/10.1016/j.oceaneng.2013.05.015

Zhang H, Jiang Q, Xu J (2013) Coastline extraction using support vector machine from remote sensing image. J Multimed 8(2):175–182. https://doi.org/10.4304/jmm.8.2.175-182

Authors and Affiliations

**Benoit Laignel[1] · Stefano Vignudelli[2] · Rafael Almar[3] · Mélanie Becker[4] ·
Abderrahim Bentamy[5] · Jérôme Benveniste[6] · Florence Birol[3] · Frédéric Frappart[7] ·
Deborah Idier[8] · Edward Salameh[1] · Marcello Passaro[9] · Melisa Menende[10] ·
Marc Simard[11] · Emma Imen Turki[1] · Charles Verpoorter[12]**

[1]   Université de Rouen Normandie, Université Caen Normandie, CNRS, M2C, UMR 6143,
      76000 Rouen, France

[2]   Consiglio Nazionale delle Ricerche (CNR-IBF), Via Moruzzi 1, 56127 Pisa, Italy

[3]   Université de Toulouse, LEGOS (CNES/CNRS/IRD/UPS), 31400 Toulouse, France

[4]   LIENSs, UMRi 7266 CNRS-La Rochelle Université, 17000 La Rochelle, France

[5]   Laboratoire Spatial et Interfaces Air-Mer (IFREMER), Centre Bretagne - ZI de la Pointe du
      Diable, CS 10070, 29280 Plouzané, France

[6]   European Space Agency (ESA-ESRIN), Largo Galileo Galilei 1, 00044 Frascati, Italy

[7]   INRAE, Bordeaux Sciences Agro, UMR ISPA, Villenave d'Ornon 33882, France

[8]   BRGM, 3 Av. Claude Guillemin, 45100 Orléans, France

[9]   Deutsches Geodätisches Forschungsinstitut der Technischen Universität München, Arcisstraße 21,
      80333 Munich, Germany

[10] IHCantabria - Instituto de Hidráulica Ambiental de la Universidad de Cantabria, 39011 Santander,
      Spain

[11] Jet Propulsion Laboratory, California Institute of Technology, 4800 Oak Grove, Pasadena,
      CA 91109, USA

[12] Université du Littoral Côte d'Opale, CNRS, Univ. Lille, IRD, UMR 8187 - LOG - Laboratoire
      d'Océanologie et de Géosciences, 62930 Wimereux, France